biosensors

MDPI

Review

A Comprehensive Review on Upconversion Nanomaterials-Based Fluorescent Sensor for Environment, Biology, Food and Medicine Applications

Wei Jiang [1], Jiaqi Yi [1], Xiaoshuang Li [1], Fei He [2], Na Niu [1,2,*] and Ligang Chen [1,*]

[1] College of Chemistry, Chemical Engineering and Resource Utilization, Key Laboratory of Forest Plant Ecology, Northeast Forestry University, 26 Hexing Road, Harbin 150040, China
[2] Key Laboratory of Superlight Materials and Surface Technology, Ministry of Education, College of Materials Science and Chemical Engineering, Harbin Engineering University, Harbin 150001, China
* Correspondence: niuna@nefu.edu.cn (N.N.); analchem@nefu.edu.cn (L.C.)

Abstract: Near-infrared-excited upconversion nanoparticles (UCNPs) have multicolor emissions, a low auto-fluorescence background, a high chemical stability, and a long fluorescence lifetime. The fluorescent probes based on UCNPs have achieved great success in the analysis of different samples. Here, we presented the research results of UCNPs probes utilized in analytical applications including environment, biology, food and medicine in the last five years; we also introduced the design and construction of upconversion optical sensing platforms. Future trends and challenges of the UCNPs used in the analytical field have also been discussed with particular emphasis.

Keywords: upconversion nanoparticles; surface modification; environmental analysis; biological analysis; food and medicine analysis

Citation: Jiang, W.; Yi, J.; Li, X.; He, F.; Niu, N.; Chen, L. A Comprehensive Review on Upconversion Nanomaterials-Based Fluorescent Sensor for Environment, Biology, Food and Medicine Applications. *Biosensors* **2022**, *12*, 1036. https://doi.org/10.3390/bios12111036

Received: 26 September 2022
Accepted: 14 November 2022
Published: 17 November 2022

1. Introduction

In 1959, Bloemberge et al. excited ZnS with 960 nm infrared and obtained its emission peak at 525 nm. Later, in 1961, Auzel observed two-photon excitation of fluorescence in Eu^{3+} doped crystals under high-power laser irradiation. Since then, the conjecture that energy may transfer between two rare-earth ions has been deeply rooted in the work of researchers. It was not until 1966, when phosphors doped with rare-earth ions were successfully synthesized, that the idea of upconversion luminescence was formally proposed. After more than 60 years of research. Lanthanide-doped upconversion nanoparticles (UCNPs) have shown high luminescence efficiency due to the long lifetime of the excited state, and they have been studied by researchers from all walks of life, gaining popularity in biomarkers, contrast agents, and other technologies. Upconversion luminescence, also known as anti-Stokes luminescence, is a particular luminescence phenomenon. The wavelength of the emitted light is less than that of the exciting light [1]. Specifically, the UCNPs luminescence mechanism is based on the following process: the luminescent center absorbs two or more low-energy photons, undergoes radiation-free decay to reach the excited state energy level, and thus returns to the ground state and releases a high-energy photon. In order to efficiently realize two-photon or multi-photon processes, the excited states of the luminescent centers need to have long energy level lifetimes. Moreover, the jumps between energy levels of rare-earth ions belong to forbidden f-f jumps with long energy level lifetimes. Therefore, the upconversion luminescence mechanism study also needs to focus on the energy level leap of rare-earth ions [2,3].

As we know, the UCNPs consist of a matrix, sensitizer, and activator. Some single-doped UCNPs do not contain the sensitizer. Among them, the matrix is the central part of the UCNPs. Many studies have proved that Y^{3+}, La^{3+}, and Lu^{3+} ions are more suitable for matrix materials. The ions that are incorporated into the matrix as luminescence centers

are called activators. Rare-earth ions with abundant energy levels such as Pr^{3+}, Nd^{3+}, Sm^{3+}, Tb^{3+}, Ho^{3+}, Er^{3+}, Tm^{3+}, etc., are commonly used as UCNPs activators. Moreover, increasing the doping concentration from the single doping activator UCNPs will cause a certain degree of luminescence of reduction [4–6]. In order to improve the luminescence efficiency, in the presence of the luminescence center, another rare-earth ion is doped with a high concentration, namely, the sensitizer. Unlike other trivalent rare-earth ions, Yb^{3+} has only one excited state, which does not reduce the luminescence properties of materials, due to concentration quenching, energy transfer, and other factors. Therefore, Yb^{3+} is the most commonly used sensitizer. In general, Yb^{3+}-Er^{3+}, Yb^{3+}-Tm^{3+}, Yb^{3+}-Ho^{3+} ion pairs double-doped UCNPs have high luminescence efficiency, and the doping of different proportions of Yb ions affects the luminescence intensity and emission peak position [7] (Figure 1), becoming the focus of research in recent years.

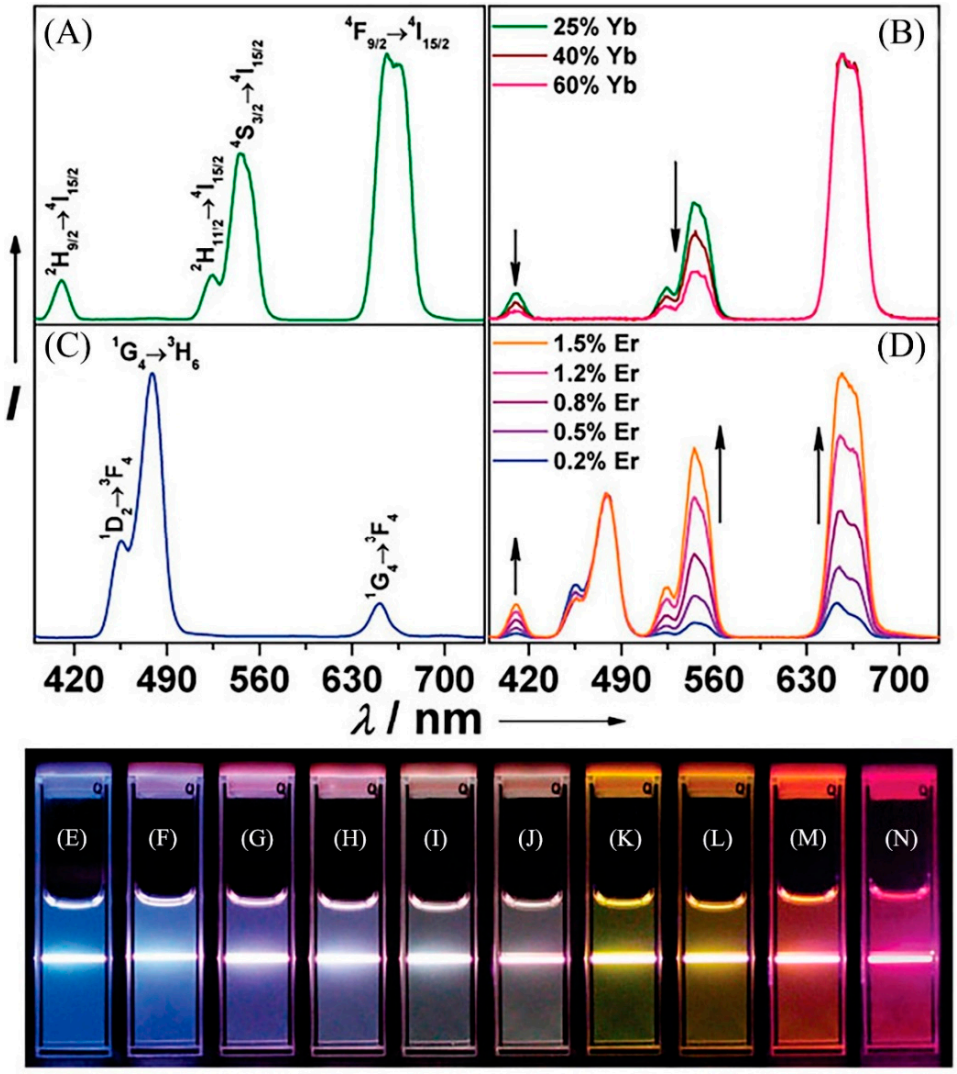

Figure 1. Room temperature upconversion emission spectra of (**A**) $NaYF_4$: Yb, Er (18/2 mol%), (**B**) $NaYF_4$: Yb, Tm (20/0.2 mol%), (**C**) $NaYF_4$: Yb, Er (25–60/2 mol%), and (**D**) $NaYF_4$: Yb, Tm, Er (20/0.2/0.2–1.5 mol%) particles in ethanol solutions (10 mM). The spectra in (**C**) and (**D**) were normalized to Er^{3+} 650 nm and Tm·480 nm emissions, respectively. Compiled luminescent photos showing corresponding colloidal solutions of (**E**) $NaYF_4$: Yb, Tm (20/0.2 mol%), (**F**–**J**) $NaYF_4$: Yb, Tm, Er (20/0.2/0.2–1.5 mol%), and (**K**–**N**) $NaYF_4$: Yb, Er (18–60/2 mol%). The samples were excited at 980 nm with a 600 mW diode laser. The photographs were taken with exposure times of 3.2 s for (**E**–**I**) and 10 s for (**M**,**N**). Reprinted with permission from [7], copyright 2008, American Chemical Society.

Although Atomic Absorption Spectrometry (AAS) [8,9], High-Performance Liquid Chromatography (HPLC) [10,11] or Mass Spectrum [12] and other instrumental analytical methods have been widely used in the analysis of metal ion, liquid organic pollutant or other substances, their expensive analytical costs and limitations in real-time detection are determined by the environment in which they are used. In contrast, fluorescence methods such as organic dyes [13], quantum dots (QDs) [14], metal complexes [15] offer the advantages of simplicity of operation, high stability, rapidity and accuracy, and the possibility of real-time detection. Among them are UCNPs, with their specific light-emitting pattern forming their unique characteristics, such as narrow emission bandwidths, large anti-Stokes shift, multicolor emission, low auto-fluorescence background, long lifetime, and high penetration stability [16]. A large number of researchers have found that these properties of the UCNPs can be put to excellent use in analytical application studies. Moreover, UCNPs have low toxicity and good chemical stability, which can make up for the shortcomings of the above-mentioned fluorescent materials in analytical applications. More importantly, the UCNPs are easily functionalized and can be applied in various fields. In this paper, we will detail the contribution of UCNPs applied to chemical analysis. Furthermore, we attempt to summarize the fluorescent characteristics and sensing applications of UCNPs in systematic mean (Figure 2).

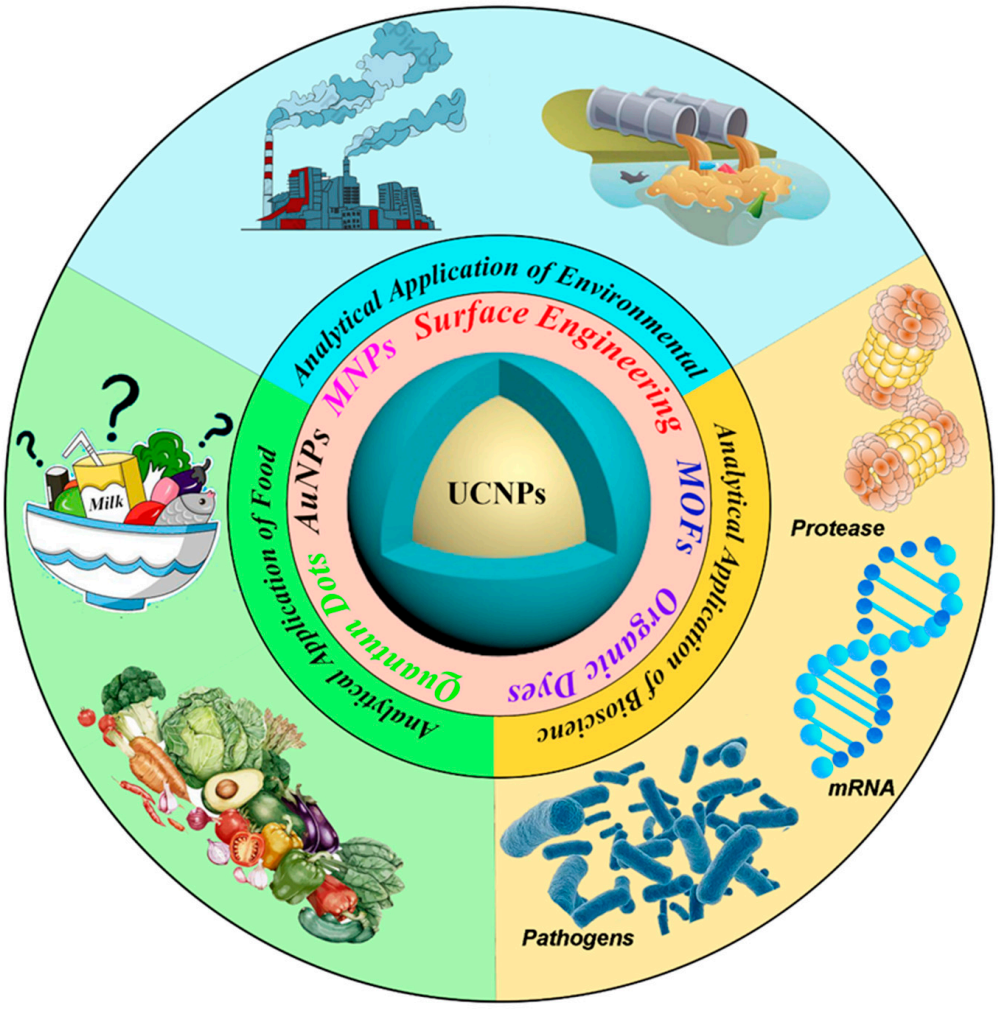

Figure 2. Schematic illustration of the fluorescent characteristics and sensing application of the UCNPs.

This review provides an overview of recent advances in the design and application of UCNPs, focusing on four distinct areas including environmental analysis, biological

analysis, food analysis, and medicine analysis. It covers sensors and assays mostly based on the UCNPs with a small size. We first introduce the synthesis of rare-earth-doped UCNPs and the surface modification processes, then we review sensing processes mechanisms and finally focus on introducing general sensing schemes for UCNPs-based chemo-sensors and biosensors.

2. Design of the UCNPs Analysis Nanoplatform

The design of the UCNPs nanoplatforms is targeted at sensing applications. So, the synthesis of the UCNPs and the construction and working mechanism of the UCNPs nanoplatforms are a prerequisite for the development of sensing schemes.

2.1. Synthesis of the UCNPs

The different composition, crystalline shape, shape, and size of nanoparticles can affect their optical properties and potential utilization in applications in fluorescence analysis or other research fields. Therefore, its synthesis methods have received much attention. In this paper, we will introduce several commonly used synthesis methods such as high-temperature pyrolysis, hydrothermal synthesis, and solvothermal methods, etc. Here, we focus more on applying the UCNPs in the analysis field, so in this chapter, we describe more synthetic methods used in recent years of applications. Researchers can choose different synthesis methods for the preparation of the UCNPs according to the diverse needs of the application (Table 1).

2.1.1. High-Temperature Decomposition Method

High-temperature pyrolysis is one of the most common methods to synthesize rare-earth UCNPs. The process involves the rare-earth precursors being dissolved in a high boiling point organic solvent and then treating them at high temperature in the presence of a surfactant for a certain period to obtain rare-earth nanoparticles with uniform morphology and controlled size. The rare-earth trifluoroacetic acid or rare-earth chloride are used as precursors, and oleic acid (OA), oleylamines, or octadecenoic with long chains and polar ends are commonly used as surfactants [17–19]. Using trifluoroacetate as the precursor, Chow et al. [20] used oleylamine solvent to prepare the 10 nm $NaYF_4$: Yb, Er. Furthermore, different reaction times, reaction reagent volume, and different reaction temperatures will affect the size and morphology of the UCNPs. While the incorporation of oily surfactants in the synthesis process poses difficulties for the application of UCNPs in analytical or biological fields, research on surface modification or functionalized UCNPs has become popular and important.

2.1.2. Hydrothermal Method

In contrast, the synthesis conditions of the hydrothermal method are more uncomplicated. The solubility and reaction rate of the inorganic precursors are increased in a solvent system by controlling a suitable temperature and a vapor pressure above a solvent system's critical value. Then, the method of preparing UCNPs by subsequent crystallization of the dissolved precursor ions from the solvent, under high temperature and pressure conditions, is conducted. This method uses a low-cost environmental solvent, and the reaction conditions are easy to control. In the process of hydrothermal synthesis, choosing the appropriate additive with specific functional groups of nanometer particle morphology and size of the control counts a great deal. Li et al. [21] proposed a liquid–solid liquid-phase method to synthesize high-quality rare-earth fluoride nanoparticles. Many kinds of nano-micron particles with different morphology and structure have been prepared by the hydrothermal method. The additives can be used as complexing agents and structure guiding agents in the process of the formation of nano-particles. Usually, the organic additives used in the synthesis of rare-earth nanoparticles include (OA) [22–24], ethylenediaminetetraacetic acid (EDTA) [25–27], cetyltrimethylammonuim bromide (CTAB) [28,29], trisodium citrate [30,31] and so on.

2.1.3. Solvothermal Method

In solvothermal methods, simple hydrothermal methods show great potential for preparing one-dimensional rare-earth ion–doped nanowires, nanorods, or nanotubes, especially for preparing rare-earth hydroxides, when no organic additives or templates are used. For example, hydroxide nanowires, nanotubes, and nanorods can be selectively synthesized in a water system of rare-earth ions and NaOH (or KOH, $NH_3 \cdot H_2O$) under specified temperature and pH conditions [32,33]. In order to fine-tune the morphology and size of the target product, the most effective and direct strategy is to add appropriate organic active agents. On the one hand, free ion concentration affects monomer concentration and growth kinetics, while the actual free ion concentration depends on the coordination between metal ions and hydrophilic ligands. On the other hand, the selective adsorption of organic ligands on the crystal surface is beneficial to obtain controllable crystal morphology. Organic active agents include hydrophilicity and hydrophobicity. Commonly used hydrophilic surfactants include citric acid (Cit^{3+}), EDTA, polyvinylpyrrolidone (PVP) [34], CTAB, polyvinylidene (PEI) [35], polyacrylic acid (PAA) [36,37], polyphosphoric acrylate (P-PAA) and 2-aminoethyl dihydro phosphates (APE). Zhang et al. [38] used OA as a surfactant to produce homogeneous $NaYF_4$ nanorods, nanorods, and flower-shaped nanorods under different reaction conditions. In addition, OA as a surfactant can also be used to prepare rare-earth-doped nanoparticles with controllable morphology and size [39].

Table 1. Design of the UCNPs analysis nanoplatform.

Synthetic Methods	UCNPs	Precursors	Surfactant	Morphology	Size	Ref.
High-Temperature Decomposition Method	$NaYF_4$: Yb/Er	$RE(CF_3COO)_3$	OA, ODE	Spherical	10 nm–30 nm	[40]
	$NaLuF_4$: Yb, Er $NaGdF_4$: Yc, Er $LiYF_4$: Yd, Er	$RE(CF_3COO)_3$		Ship-in-a-bottle	80 nm–240 nm	[41]
	$NaYF_4$: Yb, Er $NaYF_4$: Yb, Tm	$RE(CF_3COO)_3$	Oleylamine	Hexagonal	10.5 nm	[20]
	$NaYF_4$: Yb, Er/Tm		OA, ODE	Large spheres Small spheres Rods	37.9 nm 14.0 nm Length = 60.1 nm, Width = 21.5 nm	[42]
	β-$NaYF_4$: Yb, Er/Tm	NH_4F	OA, ODE	Nanoplates and Nanospheres Nanoellipses	30 nm × 30 nm × 45 nm 30 nm 17 nm–22 nm	[43]
Hydrothermal Method	$NaYF_4$: Yb^{3+}, Er^{3+}	$NaBF_4$	OA	pH = 7 Microtubes pH = 9, Microrods and nanorods pH = 11, Microtubes	14.46 μm 10.65/0.87 μm 7.90 μm	[44]
		NH_4F		pH = 7, Submicrorods pH = 9, Submicrorods pH = 11, Submicrorods	5.53 μm 4.07 μm 0.48 μm	
		NaF		pH = 7, Microtubes pH = 9, Submicrorods pH = 11, Nanorods	5.76 μm 0.86 μm 0.65 μm	
	$NaYF_4$: Yb^{3+}, Er^{3+}		OA, OH^-	Nanobranches	1.5 μm	[45]

Table 1. *Cont.*

Synthetic Methods	UCNPs	Precursors	Surfactant	Morphology	Size	Ref.
Solvothermal Method	β-$NaLuF_4$	NaF	Aitric acid (AC)	AC = 2 mmol, regular hexagonal phase microdisks AC = 3 mmol, short hexagonal phase microprisms AC = 8 mmol, hexagonal phase microtubes with hollow	Height: 0.79 μm Diameter: 7.58 μm Height: 2.12 μm Diameter: 8.51 μm Height: 9.47 μm Diameter: 1.88 μm	[46]
	$NaGdF_4$: Yb^{3+}, Er^{3+}	NaF	CTAB	Flower-like assemblies	200 nm–250 nm	[47]
	$NaYF_4$: Yb, Er@$NaYF_4$	NH_4F	OA, ODE	Hexagonal nanoparticles	9 nm	[32]
	$NaMF_4$	NaF, $M(NO_3)_3$	OA, OH^-	Uniformly hexagonal nanotubes	Length: 500 nm Diameter: 250 nm	[38]

2.2. Surface Modification Strategies for the UCNPs

As noted above, our prepared UCNPs are dispersed in organic solvents such as cyclohexane and toluene due to the surface coating by OA or oleylamine, which can cause difficulties in subsequent studies. For example, as anti-Stokes fluorescent materials with near-infrared excitation and visible light emission, the UCNPs hydrophobic surfaces need to be converted to hydrophilic surfaces for analytical assays to be performed, then to graft-specific responsive, functional groups on the hydrophilic surface for the needs of the analyte. The hydrophilic process of the UCNPs was divided into ligand-free conversion and ligand modification. In ligand-free modifications, a good example is the acid treatment method used by Nicoleta Bogdan et al. [48], whereby Oleate-capped Ln-UCNPs were dispersed in an aqueous solution, and the pH was adjusted to 4 with HCL (0.1 mol L^{-1}) to protonate the carboxylic acid group of the OA ligand (to produce OA). The UCNPs were obtained by extraction of the dispersed in water, while according to the study, the integrated UCNPs red-green emission ratio of Ln-UCNPs dispersed in toluene differs somewhat from that of Ln-UCNPs spread in water, which can be adjusted depending on the needs by adjusting the pH or by taking isotopic electronic isotopic [49]. The proposed scheme for the acid–base reaction occurring at the surface of the Ln-UCNP is as follows [48]:

$$\mathrm{LnOA}\frac{\mathrm{HCl}}{\mathrm{pH4}} \rightarrow \mathrm{LnOH} + \mathrm{OAH} \rightarrow \left[\mathrm{LnOH_2}^+\right] \cdots \mathrm{Cl}^- \quad (1)$$

$$\mathrm{LnOA}\frac{\mathrm{HCl}}{\mathrm{pH4}} \rightarrow \mathrm{LnOH} + \mathrm{OAH}\overrightarrow{\mathrm{pH7.4}}\left[\mathrm{LnO}^-\right] \cdots \mathrm{H_3O}^+ \quad (2)$$

In addition to the "ligand-free hydrophilic modification" process described above, ligand modification can be divided into organic ligands (-NH_2, -COOH) and inorganic ligands (UCNPs@SiO_2). The typical method for conversion of compounding of UCNPs@SiO_2 is Stober's reverse microemulsion method [50]. The approach is to form a water-in-oil microemulsion by adding the surfactant Igepal CO-520. After stirring, Igepal CO-520 and ammonium hydroxide were added again. Ultrasonication was performed to distribute the nanocrystals within the micelles uniformly. After adding TEOS and stirring for two days, organic solvents such as acetone were added to precipitate and separate the nanoparticles. Another surface silanization method is by adding ethyl orthosilicate dropwise (TEOS), at 70 °C, under alkaline conditions after 12 h of emulsification by adding the surfactant CTAB [51]. Different thickness of the silica shell (3–5 nm) affects the luminescence of the UCNPs to some extent, and the thickness of the shell layer can be controlled according to

the application's requirements. Although the coated silica can make the UCNPs surface hydrophilic, it does not provide the functional groups which the analyzed application process is coupled. Functionalization of the UCNPs organic ligands based on encapsulated silica is an essential part of the design of the UCNPs analysis platforms.

Table 2 illustrates some of the commonly used amination, carboxylation, and other surface modification UCNPs studies, usually the synthesis of amination UCNPs based on silylation, which is commonly performed by UCNPs of APTES or PEI grafting. In contrast, carboxylation sometimes does not require the process of silylation. However, some experiments will also be activated after the amination UCNPs and then connected to the carboxyl group. The table mentions some bioimaging or drug delivery (therapeutic) processes on the functionalization of UCNPs is hoped to bring analytical work. The functionalization of UCNPs for some bioimaging or drug-loaded (therapeutic) processes mentioned in the table is intended to inspire targeted functionalized UCNPs in some specific environments, such as He et al. [52] combined two representative biocompatible PCL and hydrophilic HPG on the UCNPs surface. Similarly, to improve the aggregation, precipitation, or degradation of the UCNPs in acidic, alkaline, or high ionic strength media, Markl et al. [32] designed self-assembling phospholipid bilayers (PLMs) functionalization $NaYF_4$: Yb, Er, which can prevent instability in phosphate-buffered solution effectively, and it is a better application for in vivo analysis of organisms.

2.3. Construction of the UCNPs Nano-Platforms

It is well known that the UCNPs have a significant anti-Stokes shift and brilliant biocompatibility. While depending on the choice of the analyte, sometimes $NaLnF_4$: Yb, Er (Tm) or another alone cannot achieve the purpose. However, the addition of two or more nanomaterials or biomaterials can help us achieve the purpose of analysis. For example, the absorption wave of gold nanoparticles overlaps with the emission spectrum of the UCNPs, which will affect the luminescence of part of the UCNPs [33]. Furthermore, gold nanoparticles are easy to modify the surface functional groups, so when analyzing different targets, fluorescence analysis can be carried out according to the different effects of the functional groups without affecting the fluorescence of the UCNPs. At the same time, in order to circumvent the problems of low-fluorescence resonance energy transfer (FRET) luminescence efficiency and low sensor sensitivity, targeted modification of the UCNPs has been an essential part of designing sensing platforms and is widely used in the analysis of metal ions and organic reagents as well [53,54]. In addition, also used is the coupling of biological elements such as antibodies, aptamers, and cDNAs using UCNPs and synergistic effects with carbon dots and graphene oxide quantum dots to analyze and detect microorganisms or small molecules such as fungal toxins [55–57] (Figure 3).

With the continuous optimization of magnetic separation technology, when the UCNPs are applied to the analysis of a specific environment, magnetic nanoparticles such as Fe_3O_4 synergize with them at the end of the analysis to facilitate the separation of the probe and the substance to be measured and facilitate the integration of enrichment and detection. Furthermore, the synergistic effect of some particles is to enhance the upconversion luminescence intensity and thus improve the detection efficiency, such as doping core–shell $NaGdF_4$: Yb, Er@$NaYF_4$: Yb^{3+}, fluorescence enhancement more than $NaLnF_4$: Yb, Er 1.6 times [58]. In addition, molecularly imprinted polymers (MIPs) molecular imprinting techniques have been combined with UCNPs to improve selectivity by exploiting the specific adsorption sites of molecularly imprinted polymers, thereby enhancing detection efficiency [59–61]. Apart from these, organic dyes [62] and fluorescein [63] are also used to form nano-fluorescent probes in synergy with UCNPs, and the applicable fluorescein is selected according to some unique properties of different substances to be measured. For example, in order to design a fluorescent probe for the detection of cysteine, Guan's group [64] used probe 5 (6)-carboxy fluorescein-O, O′-diacrylate, which has a sensitive response to cysteine (Cys), combined with the effect on the position of the upconverted emission peak to achieve the purpose of analysis.

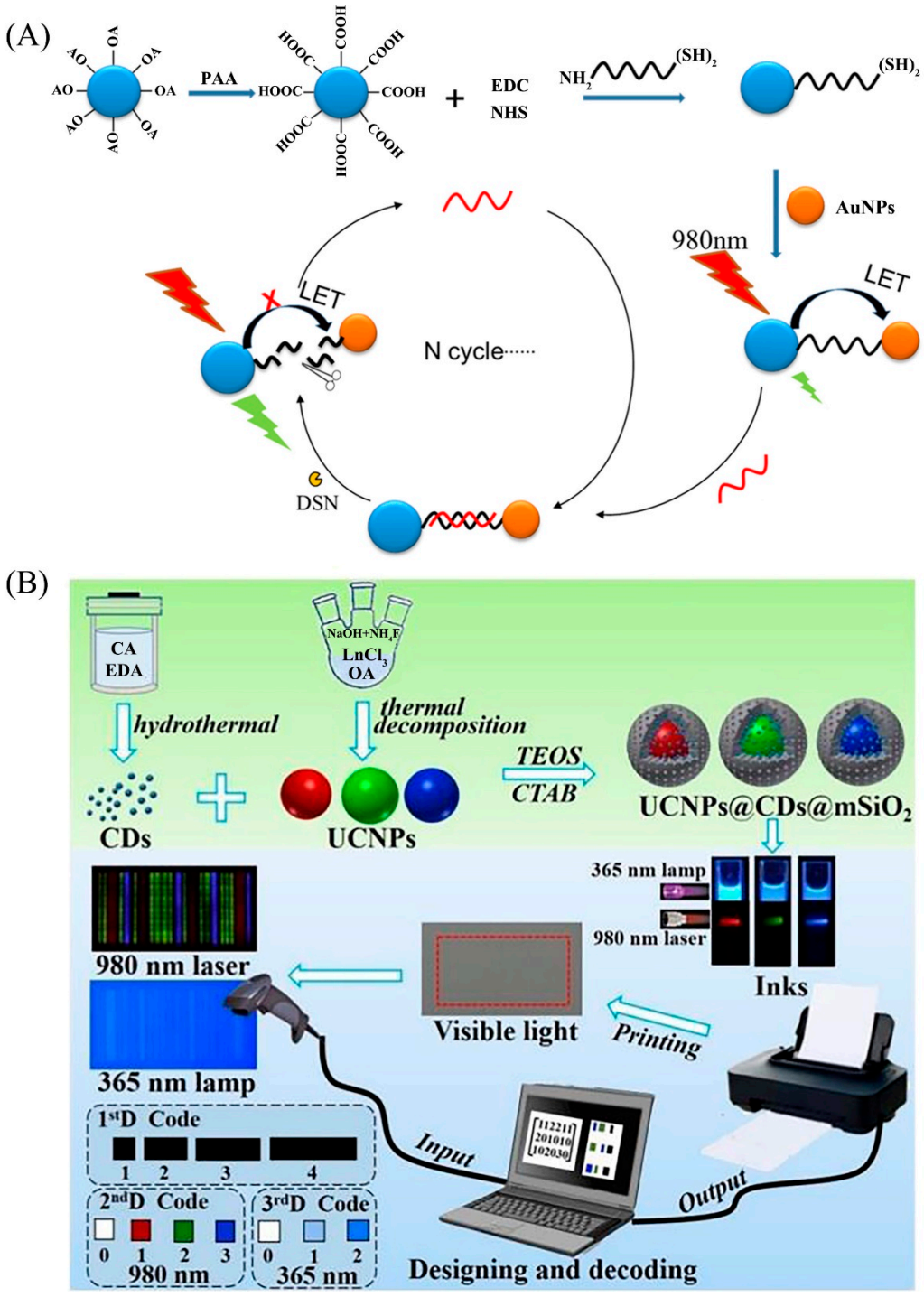

Figure 3. Schematic illustration based on the UCNPs analysis platform construction. (**A**) Schematic representation of UCNPs-AuNPs detection of miRNA155. (**B**) Schematic of both synthesis details and dual-mode fluorescence/color properties of sandwiched UCNPs@CDs@mSiO$_2$ Core-Shell nanohybrids for anti-counterfeiting barcodes. Reprinted with permission from [33,56]. Copyright 2019, Elsevier and 2019, American Chemical Society.

The design of the UCNPs nano-fluorescent probes for analytical assays has become a topical issue today. The selection of suitable structures of synergistic substances according to the requirements is still a challenging task that requires a lot of exploratory work researchers to subsequently develop innovative UCNPs fluorescent probes.

Table 2. Upconversion modifications and surface functionalization.

The UCNPs	Organic Ligands	Modified Material	Modified Purpose	Fluorescence Sensing Platform	Applications	Ref.
$NaYF_4$: Yb, Tm	NH_2-	3-aminoprop-yltriethoxysilane (APTES)	Coupling with aptamer	$NaYF_4$: Yb, Tm-NH_2/aptamer and SYBR Green-I	Oxytetracycline detecting	[65]
$NaYF_4$: Yb, Tm		APTES	Coupling with aptamer	$NaYF_4$: Yb, Tm-NH_2@ Molecularly Imprinted Polymer-aptamer	Enrofloxacin detecting	[66]
$NaYF_4$: Yb, Er@$NaGdF_4$		APTES	Activate drug delivery	$NaYF_4$: Yb, Er@$NaGdF_4$	Intracellular imaging	[67]
$NaYF_4$: Yb, Er@$NaYF_4$		PEI	Hydrophilia	$NaYF_4$: Yb, Er@$NaYF_4$-NH_2/Calcium Red/Alizarin Red S	Sensing pH	[68]
$NaYF_4$: Yb, Tm		Polyethyleneimine	Hydrophilia	$NaYF_4$: Yb, Tm-NH_2	Intracellular imaging	[69]
$NaYF_4$: Yb, Er		APTES	Absorb negative charges	$NaYF_4$: Yb, Er-NH_2@SiO_2-NH_2 and AuNPs-citrate	Cyano-containing pesticides detecting	[70]
$NaYF_4$: Yb, Er@$NaYF_4$		PAA in DEG	Hydrophilia	$NaYF_4$: Yb, Er@$NaYF_4$-COOH, OH	–	[71]
$NaYF_4$: Yb, Tm	COOH-	PAA in H_2O	Covalent coupling of dopamine by amidization reaction	$NaYF_4$: Yb, Tm-COOH-dopamine	Organophosphorus pesticide detecting	[72]
$NaYF_4$: Yb, Er		PAA in ethyl alcohol	Coupling with hydrophilic materials	$NaYF_4$: Yb, Er-COOH-RGB inks	Drug Anti-Counterfeiting	[73]
$NaYF_4$: Yb, Er (Tm or Ho)		Lemieux-von Rudloff reagent (OA is oxidized)	Coupling with proteins	UCNPs-Strepta-vidin	DNA detecting	[22]
$NaYF_4$: Yb, Tm		Methacrylic acid (MAA)	Loading CDDP	$NaYF_4$: Yb, Tm-COOH	Drug delivery	[74]
$NaYF_4$: Yb,Er		Adipic acid	Coupling the growth and hydrophilia	$NaYF_4$: Yb, Er-COOH	Intracellular imaging in vitro	[75]
$NaYF_4$: Yb, Tm	COOHCOOH	PAA in diethylene glycol	Coupling with antibody	$NaYF_4$: Yb,Tm-COOH/Magnetic polystyrene microspheres	Bisphenol A detecting	[76]
$NaYF_4$: Yb,Er	–	Poly-MAEP	Coupling with proteins	$NaYF_4$: Yb, Er-MAEP	Cell imaging	[77]
$NaLuF_4$: Yb, Er	–	Amphiphilic phospholipid functionalized poly ethylene glycol and DSPE-PEG	Amphipathy	$NaLuF_4$: Yb, Er-ph-PEG, DSPE-PEG	Deep-tissue bioimaging	[78]
$NaYF_4$: Yb, Er	Aryl group-	Phosphoryl-functionalized pillar arene	Hydrophilia	$NaYF_4$: Yb, Er-PP5	pH-responsive DDS	[79]
$NaYF_4$: Yb, Er	–	α-Cyclodextrin	Hydrophilia and specific recognize Cys	α-CD-$NaYF_4$: Yb, Er-rhodamine-oxaldehyde (RHO)	Cys detecting	[80]
LaF_3: Yb, Ho or LaF_3: Yb, Er	–	Polyethylene glycol monomethyl ether	Amphipathy	LaF_3: Yb, HO/LaF_3: Yb, Er- mPEG-OH	The UCNPs epoxidation	[81]
$NaYF_4$: Yb, Er	–	Polyethylene glycol-poly (lactic-co-glycolic acid) polymer,	Positive charge and amphiphilicity	$NaYF_4$: Yb, Er- PEG-PLGA	Drug delivery	[82]
$NaYF_4$: Yb, Er, Tm	Thiazole Derivative-	α-Cyclodextrin	Hydrophilia and specific recognize Hg^{2+}	α-CD- $NaYF_4$: Yb, Er, Tm	Hg^{2+} detecting	[83]

2.4. Mechanisms and Techniques for Optical Analysis of UCNPs Nano-Platforms in Practical Applications

Until now, The UCNPs emits high-energy visible light by two-photon or multi-photon processes under excitation with low-energy excitation light such as near infrared, which

means that upconversion nanomaterials reduce background fluorescence and light scattering [84–86], thus allowing qualitative analysis with quantitative processes that have unpredictable effects and receive increasing attention from researchers [6]. In addition, the UCNPs with long fluorescence lifetime, high quantum yield, and low photodegradation have been widely used in therapeutic, environmental, biological, food, and medical applications [87,88].

UCNPs fluorescence probes combined with fluorescence analysis are often used in material analysis to use their luminescent properties. Fluorescent determination often utilizes fluorescence labeling or label-free fluorescence techniques [89,90]. The fluorescence labeling method presupposes labeling and separation of the sample from the target analyte, and the label-free fluorescence techniques are accomplished primarily by quenching, reducing, or restoring fluorescence affected by the analyte.

The fluorescence quenching (FQ) mechanisms are mainly as follows: (i) Static or dynamic quenching: weak binding between the ground state fluorescence molecule and quench agent produce new complex, which causes the static quenching; the excited fluorescent molecule collides with quench agent which causes the dynamic quenching. (ii) Energy transfer (ET): the two standard UCNPs fluorescence sensor energy transfer modes are FRET theory, and luminescence resonance energy transfer (LRET). These mechanisms describe ET from a donor fluorophore to an acceptor fluorophore through nonradiative dipole–dipole coupling. UCNPs are used as energy donors in ordinary, and it offers considerably greater freedom for upconverted emission wavelengths than the one produced merely by the lanthanide ions. Despite there being little difference between FRET and LRET, the energy transfer in LERT is radiative, whereas it is nonradiative for FRET, and the sensitivity and selectivity of the UCNPs fluorescent probe will not be influenced by this. (iii) The Inner filter effect (IFE) refers to the absorption of the exciting radiation and/or emitted fluorescence radiation of fluorophores by absorbers in the detection system. IFE only occurs effectively if the absorption band of absorbers possesses the complementary overlap with the excitation and/or emission bands of fluorophores. This theory depends on luminescent groups that can be applied in substance analysis [91]. Compared with those fluorescence probes that can be changed directly or indirectly through surface modification or functionalization, either independent transfer of the energy or the substance to be measured, the IFE-based approach does not require the link of absorbers with fluorophores, which offers considerable flexibility and more simplicity. (iv) Photoinduced electron transfer (PET) system when upon near-infrared excitation, the excited photoelectrons of UCNPs can be captured by electron acceptors. The maximal difference between PET and FRET is that two disparate fluorescent substances pass the energy in FRET, while PET only needs a vacancy in the fluorescent group to support electron transition, which can make the operation easier [92].

Amidst label-free fluorescence techniques, biological means purpose to FQ has been applied to analysis currently, except fluorescence quenching caused by physical factors such as immunofluorescence and nucleic acid aptamer unlabeled fluorescence. Indeed, the principles of these technologies are still inseparable from physical factors. The mechanism of label-free immunoassay is that the recognition process of antibody and antigen binds or separates with the fluorescent probe competitively, and then attenuation the fluorescence signal. Similarly, the unlabeled fluorescence detection mechanism of the aptamer is that the combination of the aptamer and the target changes the secondary structure of the aptamer. Furthermore, the competitive hybridization between the complementary sequence and the aptamer changes the environment around the aptamer and weakens the fluorescence signal of the fluorescent probe.

In addition to label-free fluorescence techniques used frequently for biological detection, the above-mentioned free-labeled fluorescence technique is usually characterized through fluorescence quenching. There are other kinds of analysis modes such as ratio fluorescent analysis and Colorimetric fluorescent detection [93]. In the upconversion fluorescent probe system, the solid electron-withdrawing group connected with the UCNPs and the strong electron-donating group or electron-donating organic dye connected with

gold nanoparticles or quantum dots form a D-π-A conjugated system. During stimulation, donor-to-donor electron transfer is likely to occur, resulting in changes in fluorescence properties that can be implemented in the fluorescence signal transmission ratio test [94].

3. The UCNPs in Analytical Application of Environmental Science

The healthy water-cleaned soil and pure air in the natural environment are the cornerstone of the social environment, which is the human pursuit. Nevertheless, the progress of science and technology and the development of society also have related costs. There are heavy metal ions, organic pollutants, and waste residue in lakes and land; colored gas remains for a long time. Researchers have studied various effective methods for analyzing these ingredients, such as chromatography, which has high separation efficiency and poor qualitative ability. Moreover, mass spectrometry (MS) can detect organic compounds' structural while because of complex samples to be tested, MS alone cannot meet the requirement of testing. The development of nanotechnology, due to the size of the nanoparticles' advantages of luminescence properties, promotes the application of fluorescence detection, gradual development of nanometer fluorescent probes for analysis of toxic and harmful substances in the environment bring innovation. At the same time, compared with the expensive instrument analysis of the complex operation and strict sample pretreatment, nano fluorescent probe with simple operation and strong specificity supplies a mean for real-time detection.

The UCNPs as light-emitting tunable fluorescence sensors play a favorable role in monitoring pesticide residues, heavy metal ions, organic pollutants. Additionally, inorganic salt ions in water and soil, as well as harmful gases in the atmosphere [95–97]. Furthermore, we summarize the contribution of the UCNPs fluorescent nanoplatforms in environmental analysis in Table 3.

3.1. Organic Contaminant Residue Analysis

Common organic pollutants in the environment include organic pesticides, polycyclic aromatic hydrocarbons, dioxin compounds, polychlorinated biphenyls, phenolic compounds, etc. They are difficult to be degraded and can seriously endanger human life. Gas Chromatography-Mass Spectrometry and Liquid Chromatography-Mass Spectrometry are commonly used to detect these organic pollutants, which is more costly than the UCNPs fluorescence probe analysis we presented. Among them, organic pesticides such as organochlorine, organophosphorus, nitromethyl, and nicotine act on various crops by different toxic mechanisms. Take organophosphorus pesticides as an example, they inhibit acetylcholinesterase activity in the central and peripheral nervous system. While poisoning insects, their residues can affect human health. This chapter focuses on applying the UCNPs fluorescence analysis mainly in environmental wastewater, industrial effluents, soil contamination, etc.

Table 3. A summary of achievements in analysis of pollutants in environmental science through UCNPs platform.

Analyte	Matrix	Analysis Platform	Technique	Linear Detection Range (ng mL^{-1})	LOD (nmol L^{-1})	Recovery (%)	RSD (%)	Ref.
Metribuzin	Surface and ground waters	$NaYF_4$: Yb, Er-Near Infrared dye	Ratiometric and colorimetric	4.93 × 10–3.21 × 10^2	68	–	1	[98]
	Tap water, river water	$NaYF_4$: Yb, Er-tetramethylrhodamine	Fluorescence turn on-off	0–80	2.19×10^{-7}	91.0–115.0	2.3–3.7	[99]
Bisphenol A	Water sample	$NaYF_4$: Yb, Er@Mn-aptamer	Electrogenerated chemiluminescence	0.05–100	1.62×10^{-7}	98–102.50	–	[100]

Table 3. *Cont.*

Analyte	Matrix	Analysis Platform	Technique	Linear Detection Range (ng mL^{-1})	LOD (nmol L^{-1})	Recovery (%)	RSD (%)	Ref.
	River water	$NaYF_4$: Yb, Tm-MPMs [1]	Immunofluorescence	1×10^5–5×10^8	8.76×10^{-3}	85.35–108.35	–	[76]
Perfluorooctane sulfonate	Surface water	$NaYF_4$: Yb, Er-BSTFA [2]	Fluorescence quenching	1.5×10^3–5×10^4	2.43	85.8–118.6	9.8	[101]
Polychlorinated biphenyls	Water and soil samples	$NaYF_4$: Yb, Er-BHQ [3]-1, Carboxylated MMPs [4]	Fluorescence turn on-off	0.004–800	1.36×10^{-8}	93.4–109.7 83.2–118.5	1.6–2.9, 2.1–3.2	[102]
Ag^+	Environmental water	$NaYF_4$: Yb, Er/GQD [5]	Fluorescence turn on-off	0.022 1–107.8	0.060	95–102	2.30–3.39	[103]
Cr^{3+}	Industrial waste water	$LiYF_4$: Yb, Ho@LiYF4@Ce^{3+}	Ratiometric fluorescence	260–2600	4.1×10^2	95.7–97.2	–	[104]
Fe^{3+}	Waste water	$NaYF_4$: Gd Yb, Ho/EPA [6]	Ratiometric fluorescence	14–2800	2.5×10^2	100.9–107.3	0.8–1.4	[105]
	–	$LiYF_4$: Yb, Er, Ho, Tm@$LiYF_4$: Yb	Fluorescence quenching	0–8.6×10^6	–	–	–	[106]
Pb^{2+}	–	$NaYF_4$: Yb, Er@$NaYF_4$/AuNPs	Fluorescence turn on-off	0–4.1	4.1	–	–	[107]
	Waste water	$NaYF_4$: Gd, Yb, Ho/MNPs/AuNPs	Fluorescence turn on-off	2.05–114.8	5.7	99.6–105.2	0.9–2.2	[57]
Cu^{2+}	Tap water	$NaYF_4$: Yb, Er/ AuNPs-4-mercaptobenzoic acid	Fluorescence turn on-off	1.28–64	18.2	98–106	1.2–1.8	[108]
PO_4^{3-}	Aqueous samples	ZrO_2: Yb, Er@ZrO_2/ Fast Green alimentary dye	Fluorescence turn on-off	1.9–95	20	–	–	[109]
SO_2	SO_2 gas in atmosphere	$NaYF_4$@$NaYF_4$: Yb, Tm/ cyanine dye	Fluorescence turn on-off	1×10^{-3}–1×10^3	1.6×10^{-2}	–	–	[110]

[1] MPMs: magnetic polystyrene microspheres; [2] BSTFA: N, O-bis(trimethylsilyl) trifluoroacetamide; [3] BHQ: quenchers; [4] MMPs: magnetic microspheres; [5] GQDs: graphene quantum dots; [6] EPA: N, N-diethyl-p-phenylenediamine.

Organic herbicide processes forceful systemic, which can produce targeted toxicity. Although OCs have self-decomposition ability, their residual toxicity can last a long time. Sayed M. Saleh et al. [98] designed a ratiometric and colorimetric optical sensor film which consists of near-infrared (NIR) dye 2-[2-[2-Chloro-3-[2-[1, 3-dihydro-3, 3-dimethyl-1-(4-sulfobutyl)-2H-indol-2-ylidene]-ethylidene]-1-cyclopenten-1-yl]-ethenyl]-3, 3-dimethyl-1-(4-sulfobutyl) -3H-indolium hydroxide and UCNPs, making use of UCNPs can be emitted a dual (green and red) emission under 980 nm laser diode excitation. The NIR probe conjugated system has a chloro group to the nucleophilic substitution of amines which changing the electronic distribution of their conjugated system causes the difference fluorescence signal. Then, the metribuzin is to identify. This system is precise because polyvinyl chloride (PVC) polymer was utilized to provide high homogeneity protecting fluorescent probes from leaching out. The cocktail exhibits high stability over long periods of time, high reproducibility, and exposure to pesticide media exhibits high stability.

Bisphenol A, which is widely used in plastic products such as water bottles, is an environmental estrogen that can enter water or soil during plastic degradation, so bisphenol A (BPA) testing has become particularly important. Therefore, Li et al. [99] designed streptavidin and amino groups modified UCNPs, and the modification of amino groups can save the use of biological materials. Additionally, the detection limit can be as low as 0.05 ng mL^{-1}. Compared to the above method, Guo et al. [100] took advantage of an aptasensor labeled with Mn^{2+}-doped $NaYF_4$: Yb, Er combined with electrogenerated chemiluminescence, which solved the oxidation of Bisphenol A near catechin potential sensi-

tivity of analysis, which was improved. Fluorescence analysis of electroluminescence-assisted UCNPs improves the analysis speed and the detection limit is as low as 0.037 ng mL^{-1}.

Many kinds of persistent organic pollutants are so due to their persistence, bioaccumulation, high toxicity, and complex environmental degradation, such as widespread contaminant PFOS. Li et al. [101] designed a fluorescence sensor, UCNPs@COFs, through hydrogen-bond interactions between COFS and PFOS to quench the UCNPs fluorescence. At the same time, COFS on the surface of UCNPs is ready to improve the fluorescence quantum yields and cause the sensor much more sensitivity. Tian et al. [111] prepared $NaYF_4$: Yb, Er@$NaGdF_4$@MIP to detect PFOS, and this fluorescent sensing can be used in a wide range of applications without affecting the upconversion of luminescence during specific identification.

Wang et al. [102] prepared a UCNPs fluorescent aptasensor based on hybridization chain reaction and nicking endonuclease. This aptasensor has been developed to detect polychlorinated biphenyls. The robust aptasensor can be applied for the analysis of actual samples, and it also has high sensitivity and excellent selectivity (Figure 4).

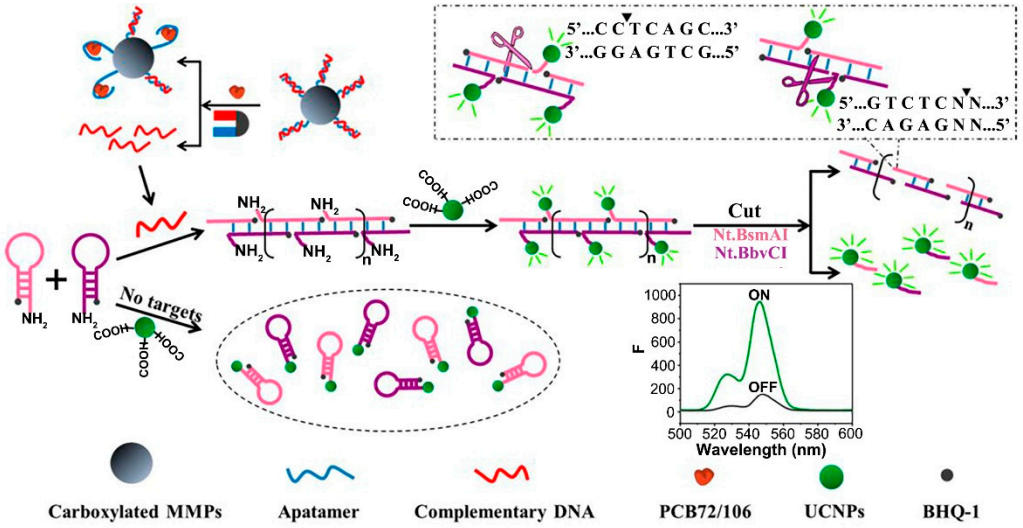

Figure 4. Schematic illustration of the dual-amplification strategy for PCB72/106 detection of upconversion fluorescent aptasensor based on HCR and nicking endonuclease. Reprinted with permission from [102]. Copyright 2018, American Chemical Society.

The UCNPs have favorable biocompatibility, stably coupling with nuclein and amino acids to use a fluorescence immunoassay in organic pollutants analysis. Duan et al. [76] proposed a fluorescence immunoassay sensor to detect BPA with anti-BPA antibody conjugated carboxyl functionalized the UCNPs and coating antigen-conjugated carboxyl-functionalized magnetic polystyrene microspheres. This method can provide a suitable way for quick field analysis, which can be very accurate.

3.2. Inorganic Contaminant Analysis

In this section, we summarized recent works on the use of UCNPs for detecting various inorganic contaminants such as chemical ions. Moreover, the results also deliver real-time information on targeted ions in complex samples, and some gas pollutants.

3.2.1. Heavy Metal Ion Analysis

Toxic heavy metals such as Chromium (Cr), Iron (Fe), Copper (Cu), Lead (Pb), Silver (Ag), and Mercury (Hg) are increasing discarded into environmental surroundings such as soil, river, lake, and pond water. What is more serious is that toxic heavy metals pose a threat to human existence indirectly. These metal ions can be analyzed explicitly in the light of luminous intensity changes in UCNPs, including luminescence enhancement, luminescence attenuation, and fluorescence quenching.

Among the rest, silver ions have excellent antibacterial activity, but a heavy metal contaminant can also cause irresistible side effects in humans. In 2017, He et al. [103], taking advantage of the ability of Ag^+ to specifically bind to two cytosines (C) mismatch in DNA to form stable C-Ag^+-C complexes, established Sodium citrate functional UCNPs and NH_2-ssDNA functional graphene quantum dots. When adding Ag^+ to this system affected by FRET, UCNPs are fluorescence quenching.

Chromium is a trace metal element of the human body for physiological function, but excessive intake of chromium ions is seriously harmful to health. Liu et al. [104] used the luminance tunability of UCNPs to design a single structure Ce^{3+}-doped $LiYF_4$: Yb^{3+}/Ho^{3+}@$LiYF_4$ modified by CRD through FRET. With the addition of Cr^{3+} into the probe solution, the color of the solution will be changed from green to other colors (Figure 5A).

3.2.2. Inorganic Acid Ion

Phosphorus is required for plants growing. Ramirez-Garcia et al. [109] designed a nano-scale conjugated fluorescence sensor. The sensor uses conjugated luminescence of Fast Green alimentary dye (FG) and ZrO_2: Yb, Er@ZrO_2, as well as the strong interaction and spontaneous formation of chemical bonds between phosphate group and zirconia (ZrO_2) as a phosphate monitor in the environment, as shown in Figure 5B. This sensor structure can enhance the upconversion luminescence, thus improving its sensitivity. While using FG, it is necessary to pay attention to its particular physical characteristics. It is therefore highly desirable to design better UCNPs-based nanosensors for PO_4^{3-}.

3.2.3. Air Pollutants

Sulfur dioxide (SO_2), nitric oxide (NO), sulfuretted hydrogen(H_2S) as a dominant component of industrial waste gas. Additionally, it has become a key indicator in the monitoring of atmospheric contamination. Zhang et al. [110] set a paper-based sensor through cyanine modified UCNPs to detect SO_2. On account of FRET between cyanine and UCNPs to decrease UCNPs luminescence, the absorption of the cyanine dye can be quenched after reacting with bisulfite ions, thereby increasing the luminescence of UCNPs.

It is sensitive to utilize test paper to monitor SO_2 when building a smartphone-based detection platform, manufactured via 3D printing technology. It provides a highly feasible idea for the real-time monitoring of other gas pollutants such as NO or H_2S.

(A)

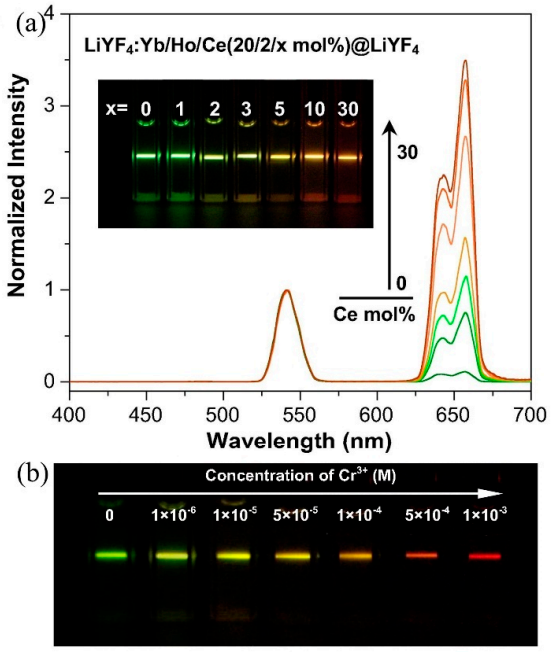

Figure 5. *Cont.*

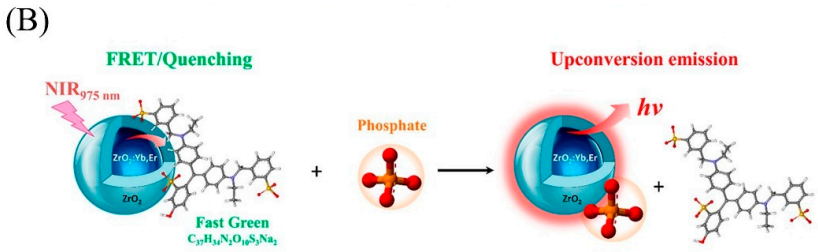

Figure 5. UCNPs for detecting heavy metal, inorganic acid ion and air pollutants. (**A**) (a) Upconversion emission spectra of the $LiYF_4$: Yb^{3+}/Ho^{3+}/Ce^{3+}(20/2/x mol%) @$LiYF_4$ as a function of Ce^{3+} content in the core. The spectra were normalized by the Ho^{3+} emission intensity at 540 nm. The inset is the corresponding luminescence photographs. (b) Typical luminescence photos of the UCNPs-CRD probe solution under the excitation of 980 nm laser (15 W cm^{-2}) at different concentrations of Cr^{3+}. (**B**) Schematic illustration of the phosphate determination method based on FRET from ZrO_2: Yb, Er@ZrO_2 core@shell nanoparticles to the FG acceptor. Reprinted with permission from [104,109]. Copyright 2017, Elsevier and 2019, American Chemical Society.

4. UCNPs in Analytical Application of Bioscience

The UCNPs have shown significance as biomarkers compared to traditional fluorescent dyes because of unique anti-Stokes fluorescence properties [112]. The excitation of UCNPs bio-labels allows NIR light, it is non-invasive, and it can penetrate deep into cells and tissues. This property of the UCNPs make its fluorescence unaffected by the sampling fluid during the detection process. More importantly, NIR irradiation is not absorbed by biological samples and therefore does not produce an auto-fluorescent background [113]. Moreover, it significantly reduces the LOD that cannot be obtained by conventional assays. Therefore, the application of UCNPs in bioanalysis has obvious advantages.

4.1. Analysis of Biomacromolecule

Biological macromolecules, including proteins, enzymes, and nucleic acid, will reflect the body's physiological state to a certain extent. Then, UCNPs, a slapping fluorescent probe, can monitor them and provide essential information for lesion diagnosis and later treatment.

4.1.1. The UCNPs Analysis of Proteins

There are three kinds of commonly used analysis strategies for UCNPs to detect protein. (i) Constructing a FRET system with other factors; (ii) The UCNPs can be used as a medium to build a hairpin DNA probe, and the premise is that the probe contains a substance which can be identified explicitly with the protein being tested. (iii) UCNPs use identified protein antibodies as vectors. Protein detection can be realized using the advantage of UCNPs biological binding, combining instruments, or constructing fluorescent side-flow biosensors.

Heparin is a polysaccharide that works as a clinical anticoagulant drug to prevent blood clotting, while heparin overdose and prolonged use could induce potentially fatal bleeding complications. Additionally, protamine is the antidote for heparin. Long et al. [114] designed the UCNPs-AuNPs FRET system formed by the electrostatic adsorption, which will quench UCNPs, because the protamine has much positive charge and it can bind to AuNPs to make UCNPs fluorescence recovery. Additionally, because heparin is electron rich, adding it to this solution will combine with protamine, and then UCNPs fluorescence will be quenched again. The sensitivity of this dual function probe is relatively high, and the detection line of heparin is decreased to 0.7 ng mL^{-1}.

Alpha fetoprotein (AFP) is an important cancer biomarker of liver cancer, currently detecting AFP relays via instrumental means. Hu et al. [115] established an immunoassay based on ICP-MS using UCNPs as elemental tags to determine AFP. The proposed method is rapid and accurate. Moreover, it has good tolerance to complex biological matrices,

indicating the great potential of UCNP as an elemental marker in biological research. Zhai et al. [116] prepared $NaYF_4$: Yb, Tm/ZnO/CdS composite film electrode by pulsed laser deposition, prompting the photoelectrochemical performance of the electrode, and more importantly it shows ultrasensitive detection of AFP. Its low detection limit can reach 5 pg mL^{-1}. It is one of the best results of all AFP analyses. A similar consequence can be achieved through the photoelectrochemical (PEC) immunoassay sensing technique. Luo et al. [117] used the high catalytic activity of glucose oxidase (GOx) to construct core–core–shell UCNP@Au@CdS and generated H_2O_2 using polyclonal anti-AFP antibodies. A sandwiched immunoreaction was first performed in microtiter plates coated with monoclonal anti-AFP antibodies. Additionally, antibody-labeled gold nanoparticles were utilized as secondary antibodies to promote photocurrent signals.

While one limitation of this method is that the generated H_2O_2 by enzyme immunoassay is artificially injected into the photocurrent detection cell, we need to simplify the process for experimental purposes.

Target-triggered DNA assembling probes labeled with UCNPs mediated amplification strategy provide more affinity sites to improve system sensitivity. Liu et al. [118] designed a target-triggered DNA assembling probe for a specific analysis of growth factor-BB. Among them, the hairpin DNA (H-DNA) probe was designed containing (a) an aptamer domain for protein recognition and (b) a blocked DNAzyme domain for DNA-zyme cleavage. Once H-DNA and A-DNA recognize the same protein, H-DNA and A-DNA are near each other. The unfolded DNAzyme hybridized with the added MB-UCNP and catalyzed the cleavage of the MB-UCNP amplification signal when Zn^{2+} is added as a cofactor.

The UCNPs probe includes two affinity sites. The target proteins binding to two affinity probes can be applied in this strategy. Such UCNPs probes can only detect specific proteins because of the limitation of relying on one or more affinity sites. If there are no affinity sites in the protein, we cannot use this method. At the same time, it is not such a suitable means for most proteins, and it will take too much time and is much expensive. A sensitive and straightforward UCNPs probe to detect growth factor-BB (PDGF-BB) will be designed, just like a direction of effort.

Some enzymes as specific proteins in organisms have a heavy response with the UCNPs fluorescent platforms, which can shred evidence to inform clinical diagnosis. Alkaline phosphatase (ALP) is a necessary serum biomarker that is an essential indicator of clinical diagnostics. Chen et al. [119] designed an enzyme cascade signal-amplified (ECSAm) strategy with label-free silver triangular nanoplates (AgTN-Ps) combined with UCNPs that can realize rapid and accurate recognition of ALP in serum, while this process is not as complex when compared with a "turn-on" sensor based on MnO_2-coated UCNPs prepared by Liang et al. [120]. Because only one reaction of ascorbic acid and MnO_2 reduction is introduced, it simplifies the operation of the experiment. The weakness of this method is that its LOD compared with the former 0.035 mU mL^{-1} is a little higher.

Bifunctional UCNPs can detect metal ions simultaneously while detecting enzymes, due to the ability of some metal ions to form complexes with enzymes, such as $(GSH)_4Cd$ complex, which is formed by the aggregation of Cd^{2+} and GSH, and Fang et al. The authors of [121] used GSH as a link to detect acetylcholinesterase (AChE) through AuNPs-UCNPs FRET sensing platform. Moreover, the detection limit of AChE activity is 0.015 mU mL^{-1}.

4.1.2. The UCNPs Analysis of Nucleic Acids

The aberrant expression of MicroRNAs (miRNA) is usually associated with human cancer. The diagnosis and discovery of miRNA at an early stage of the disease are essential. The abundance of miRNA is a little low, and PCR can amplify mRNA detection accuracy in common, while the fee is costly. Researchers use chemical methods by introducing UCNPs, which have no background autofluorescence, no photobleaching, and stable luminescence, and which detect miRNA in the cell.

In order to achieve rapid, simple, and sensitive analysis of miRNA, many researchers have designed the contact sites and structural regulation of UCNPs (Table 4).

Because RNA sequence fragment signals are pretty weak, sequence amplification is necessary, but it is complex. Many researchers are devoted to combining UCNPs FL sensors with DNA or produce devices, because it can amplify signals to achieve sensitive and speedy analysis of mRNA without amplification. This design brings many challenges to the experiment and becomes a problem to be overcome in future research.

4.2. Analysis of Small Biomolecules

Biological small molecules including amino acid and polypeptide et al. For example, the chemical structure of amino acids is easily captured by substances modified on the surface of UCNPs. Or it can be directly designed as a fluorescence resonance energy transfer IFE sensor. This has also become one of the ordinary means to detect other small biological molecules on the UCNPs nano platform.

4.2.1. The UCNPs Analysis of Amino Acid

Associated with detecting arginine, Wu et al. [122] used the guanine group in the positively charged arginine to bind to the AuNPs electrostatically to designed a FRET system between the UCNPs and AuNPs, and the limit of detection is as low as 2.9 μmol L^{-1}. Using UCNPs to analyze tyrosinase can show a dual-functional sensor, as Wang et al. [123] studied, since the tyramine under the action of tyrosinase generated melanin polymers can convert fluorescence quenching. Additionally, the fluorescence intensity has a linear relation with the concentration of tyramine. Moreover, the result has a linear relation and the activity of tyrosinase, to realize the double function test. The content of tyrosinase was measured indirectly, and the analysis of tyrosinase detection limit was as low as 0.003 U mL^{-1}.

4.2.2. The UCNPs Analysis of Peptides

Glutathione can reflect the human immune system in some conditions, and some researchers are interested in detecting it. Sun et al. [53] designed bifunctional UCNPs fluorescence probes to detect glutathione (GSH) and Cd^{2+}, and the probes have consisted of UCNPs and AuNPs. Compared with Nguyen et al. [124] utilizing Rhodamine B derivative UCNPs to detect GSH by the FRET principle, the last method is a little expensive, and this way provides a much easier choice, with no background fluorescence. Moreover, Chen et al. [125] built core–satellite UCNPs and introduced CaF_2, thus enhancing the absorbability of biomass. The key to this method is constructing the UCNPs structure by the sequential injection technique. Most importantly, it can produce specific recognition of GSH.

4.2.3. The UCNPs Analysis of Neurotransmitter

Dopamine (DA) is the most abundant catecholamine neurotransmitter in the brain. In contrast, clinical diagnosis of dopamine is often unsuitable for routine analysis, due to the high cost, long analysis time, complex pretreatment, and low selectivity to dopamine in the analysis process. Jose et al. [126] used UCNPs as a resonant light scattering (RLS) nanometer probe for quantitative analysis of dopamine, achieving trace analysis of biological samples with accurate detection data and excellent selectivity. Furthermore, Kumar et al. [127] developed a facile UCNPs sensing platform to detect DA in real time, wherein the LOD is as low as 0.63 nmol L^{-1} and the method is highly sensitive and agile (Figure 6A). Early sensitivity analyzation of thyroid-stimulating hormone (TSH) allows for early diagnosis of thyroid related disorders. Liu et al. [128] designed the UCNPs-tetramethylrhodamine (TAMRA) graft aptamers for the detection of TSH. When TSH bound to the aptamer to form a stable hairpin structure, the distance between UCNPs and TAMRA was reduced, thus causing the fluorescence quenching of $NaYF_4$: Yb, Er, so that the TSH can be detected rapidly in serum.

4.3. Analysis of Microorganism

It detects microorganisms such as fungi, mycotic, pathogens, viruses, etc., that utilize electrostatic interactions between UCNPs and microorganisms and unique fluorescence properties of UCNPs. This chapter's content lies in elaborating the application of up-conversion fluorescence analysis in the biological context. However, the collation found the detection of microorganisms in this section, and it has a pattern with the analysis of microorganisms in the food context. Then, in this section, a complete description of the UCNPs is applied to the analysis and detection of microorganisms. Chapter 5 will not be repeated. The specific content is organized as follows.

There are five patterns of microbial detection: (i) the UCNPs modified with antibodies to capture antigens assembled by magnetic nanoparticles (MNPs) or other analogs and utilizing the luminescence properties of UCNPs; (ii) the energy donor is composed of UCNPs attaching to antibodies or aptamers, and the energy receptor consisted of AuNPs or other nanoparticles or fluorescent quenchants combined with antigens or cDNA; (iii) the UCNPs as a carrier were used on the electrochemical immune analysis, and the lateral flow immune paper-based for detection is derived, which is based on the immune analysis; (iv) utilizing UCNPs luminescent signal can be adjustable to detect microbes through grafting optical fiber material or mesoporous-doped material; (v) combining with double or more modes for rapid real-time detection.

Here, the list is as follows, according to the selection of fungal toxin to be tested (Table 5).

Table 4. Summary of experimental results for miRNA detection.

Detector	Fluorescence Probe	Detection Method	Highlight	LOD	Linear Range	Ref.
mRNA	$NaGdF_4$: Yb^{3+}, Er^{3+}/AuNPs@Pt satellite assemblies	Fluorescence analysis	In situ imaging and quantification of TK1 mRNA in live cells.	0.67 fmol (10 μg RNA) $^{-1}$	1.17–65.21 fmol (10 μg RNA) $^{-1}$	[129]
miRNA-21	$NaYF_4$: Yb^{3+}, Er^{3+}-DNA H_1	Inductively coupled plasma-mass spectrometry	Sensitivity.	0.041 fmol L^{-1}	0.1–500 fmol L^{-1}	[130]
miRNAs	$NaYF_4$: Yb^{3+}, Er^{3+}-NH_2/$NaYF_4$: Yb^{3+}, Er^{3+}-COOH/dye UC	Fluorescence analysis	–	5×10^5 fmol L^{-1}	2×10^5–1.4×10^6 fmol L^{-1}	[131]
miRNA-155	$NaGdF_4$: Yb^{3+}, Er^{3+}@$NaYF_4$-DNA/AuNPs	Fluorescence analysis	–	4.5×10^3 fmol L^{-1}	0.1×10^5–1.5×10^6 fmol L^{-1}	[33]
miRNA-21, miRNA-10b	$NaYF_4$: Yb^{3+}, Tm^{3+}, Er^{3+}-Ti_3C_2	Fluorescence analysis	Assisted single-stranded replacement double-amplified RNA detection of mRNA in cell lysates without complex equipment, allowing detection of different sequences of RNA according to test requirements.	–	5–1 $\times 10^5$ fmol L^{-1}	[132]
miRNAs	CaF_2: Yb^{3+}, Ho^{3+}@MSNs@SiO_2-ssDNA/Polyurethane fibers@GO	Fluorescence analysis	Enrichment of RNA and greatly improves accuracy.	2×10^4 fmol L^{-1}	–	[133]
miRNA-21	Fe_xCu_ySe@$NaYF_4$: Yb^{3+}, Tm^{3+}	Fluorescence analysis and magnetic resonance imaging	Dual signals for in situ quantitative imaging analysis.	0.0058 amol (ng RNA)$^{-1}$	0.035–31.824 amol (ng RNA)$^{-1}$	[134]

Table 5. Microorganisms analyzed by the UCNPs nanoplatform in the last five years.

Microorganisms/ Analytes	Fluorescence Probe	Detection Mechanism	Detection Method	Linear Range (ng ml^{-1})	LOD (ng ml^{-1})	Sample	Ref.
Dipi-colinic acid	$NaYF_4$: Yb, Er-TPP [1]/EBT [2]	Luminescence	Colorimetric assay protocol	334–3.34 × 10^4	1.5 × 10^2	Human serum	[135]
Deoxynivalenol	Antibody-$NaYF_4$: Yb, Tm, Gd/Antigen-MNPs	Luminescence	Immunofl-uorescence analysis	0.001–0.1	0.001	Adulterated oil	[136]
E. coli.	cDNA-$NaYF_4$: Yb, Er/ Aptamers-AuNPs	FRET	Fluorescence analysis	5–106 (cfu mL^{-1})	3 (cfu mL^{-1})	Tap/pond water and milk	[137]
	cDNA-NaY/GdF_4: Yb, Ho/Aptamer-MNPs	Luminescence	Immunofl-uorescence analysis	58–58 × 10^6 (cfu mL^{-1})	10 (cfu mL^{-1})	Adulterated pork	[138]
	Aptamer-$NaYF_4$: Yb, Er@$NaYF_4$/WS_2 [3]	FRET	Fluorescence analysis	85–85 × 10^7 (cfu mL^{-1})	17(cfu mL^{-1})	Tap water, green tea powder	[139]
Fumonisin B1	cDNA-$NaGdF_4$: Yb, Er/AuNPs	FRET	Fluorescence analysis	1 × 10^{-5}–0.1	3 × 10^{-6}	Corn	[140]
Microcystin-LR	$NaYF_4$: Yb, Tm@$NaYF_4$: Yb-COOH/MoS_2	Luminescence	Fluorescence analysis	0.01–50	0.002	Tap water	[141]
Mycotoxins zearalenone	cDNA-$NaGdF_4$: Yb, Er/AuNPs	FRET	Fluorescence analysis	0.05–100	0.01	Corb	[140]
Ochratoxin A	$NaYF_4$: Yb, Er/GO [4]	FRET	Fluorescence analysis	0.001–250	0.001	Beer	[59]
	$NaYF_4$: Yb, Er@Mn/Fe_3O_4NPs	Luminescence	Indirect competitive immunofluores-cence analysis	–	9.553 × 10^{-3}	–	[142]
	Aptmer-$NaYF_4$: Yb, Er	Luminescence	Immunofl-uorescence analysis	5–100	1.86	Spiked wheat and beer	[143]
	$NaYF_4$: Yb, Er/AuNPs	FRET	Fluorescence analysis	0.1–1000	0.022	–	[144]
	$NaYF_4$: Yb, Tm/Polystyrene beads	Luminescence	Indirect competitive immunofluores-cence analysis	–	0.34721	–	[145]
Polymyxin B and polymyxin B-resistant bacteria	$NaGdF_4$: Yb, Er/AuNPs	Luminescence	Fluorescence analysis	–	–	Clinic urine	[146]
Single Escherichia coli	KLu_2F_7: Yb, Er/Tapered optical fiber	Luminescence	Fluorescence analysis	–	–	–	[147]
Staphylococcal Enterotoxin B	$NaGdF_4$: Yb, Er/AuNR@Pt	FRET	Fluorescence analysis	2 × 10^{-3}–0.4	0.9 × 10^{-3}	Spiked milk	[148]
	$NaGdF_4$: Yb, Er/AuNPs	Luminescence	Simultaneous detection of surface-enhanced Raman, fluorescence and circular dichroism modes	1 × 10^{-3}–0.75	–	Spiked milk	[149]
T-2 Toxin	NH_2-$NaYF_4$: Yb, Er@SiO_2/ Fe_3O_4 MNPs [5]	Luminescence	Fluorescence analysis	0.1–100	0.035	Beer	[140]
Yersinia pestis EV76	$NaYF_4$: Yb, Er	ECL [6] signal	Electrochemical immunoassay	–	1.2 × 10^4 (cfu·mL^{-1})	Soil	[150]
Listeria monocytogenes	$NaGdF_4$: Yb, Er/MNPs	Luminescence	Fluorescence analysis	68–68 × 10^6 (cfu mL^{-1})	8 (cfu mL^{-1})	Pasteurized milk	[151]
Staphylococcus aureus	$NaYF_4$: Yb, Er/AuNPs	FRET	Fluorescence analysis	47–4.7 × 10^7 (cfu mL^{-1})	10.7 (cfu mL^{-1})	Pork, beef	[152]

[1] TPP: sodium tripolyphosphate; [2] EBT: eriochrome black T; [3] WS_2: layered tungsten disulfide; [4] GO: graphene oxide; [5] MNPs: magnetic nanoparticles; [6] ECL: electrochemiluminescence.

4.4. Analysis of Inorganic Substances in Biological Samples

According to the current researchers' statistics of the research results, the UCNPs for the analysis of inorganic substances applied to biological materials can be divided into the following three categories: inorganic ions, reactive oxygen species, and gas molecules.

4.4.1. The UCNPs Analysis of Inorganic Ions in Biological Samples

Inorganic ions play a critical role in the process of life. Wei et al. [153] designed an ingenious FRET system in which Fe^{3+}-responsive Nile red derivative (NRD) was used as an energy donor, and the PEGylated amphiphilic polymer-modified UCNPs was used as energy acceptor. In addition, most of the Fe^{3+} selective probes are insoluble in water, so this structure solved this problem, and it is beneficial to the detection of Fe^{3+} in vivo, and its application in imaging has been proved (Figure 6B). Zhao et al. [154] utilized the Fenton reaction, the hydroxyl group produced when Fe^{2+} and hydrogen peroxide exists in vivo reacts with IR-808, and then the fluorescence resonance particles were increased to quantify Fe^{2+} accurately. Jiang et al. [155] improved the method of detecting Fe^{2+} in serum by designing a fluorescence sensor based on FRET between $NaYF_4$: Yb, Tm and MnO_2. After the addition of Fe^{2+}, MnO_2 was reduced to Mn^{2+}, thus restoring the fluorescence of UCNPs. Mercury ion is a potent neurotoxin that accumulates in human bodies and causes severe nervous system damage.

Then, Huang et al. [156] utilized T-Hg^{2+}-T base pairs to stabilize the two thymine (T) mismatched DNA to design DNA-functionalized upconversion nanoparticles. After adding Hg^{2+}, the fluorescence of DNA-UCNPs will be quenched.

Compared to these two methods, the structure of the former fluorescence probe is simpler and easier to operate, while the latter is significantly more complex. However, the latter has a broader range of applications. For example, it can be applied to the environment in tap water or human urine, while the former is used for cellular environmental analysis. Additionally, readers can choose appropriately according to their needs. The detection range of the former (0–8 μmol L^{-1}) is not as wide as that of the latter (10–10^4 nmol L^{-1}).

Potassium ions are electrolytes essential for homeostasis in the body. Real-time tracking of potassium concentrations in body fluids can provide important information for biomedical diagnosis, assessment of therapeutic interventions and optimization of exercise performance [157,158]. Chen et al. combined $NaYF_4$: Yb, Tm (U-Tm, blue emission) and $NaYF_4$: Yb, Er (U-Er, green emission) UCNPs with AuNP quenchers to construct two DNA-assembled nanosensors for monitoring H^+ and K^+ in the lumen of lysosomes. The different DNA-based sensor is capable of imaging both H^+ and K^+. The sensor can correlate the K^+ concentration and pH in the lumen of the lysosomes, probing during lysosomal acidification to answer important biochemical and cell biological questions [159].

4.4.2. Upconversion Analysis of Reactive Oxygen Species

Reactive oxygen species (ROS) produced through the body's metabolism, including superoxide (O_2^-), hydrogen peroxide (H_2O_2), hypochlorite (ClO^-), etc., play critical roles in many physiological processes.

Hao et al. [160] assembled a structure that analyzed ROS extensively, consisting of a UCNP core and a zeolitic imidazolate framework-8 (ZIF) shell encapsulated with chiral NiSx NPs. In vivo, H_2O_2 was successfully monitored by proportional assembly signal to verify its potential. The emission peaks of UCNPs doped with different rare-earth ions are different, and this property was to design the ratio fluorescent probes. Cy808 dye was used to enhance the luminescence of UCNPs by Zou et al. [161], and the excitation light of 808 nanometers was reduced while the excitation light of 980 nm remained unchanged after the addition of ClO^-, to realize the identification of ClO^-, which was successfully applied in mice with high sensitivity and a detection limit of 3.6 nmol L^{-1}.

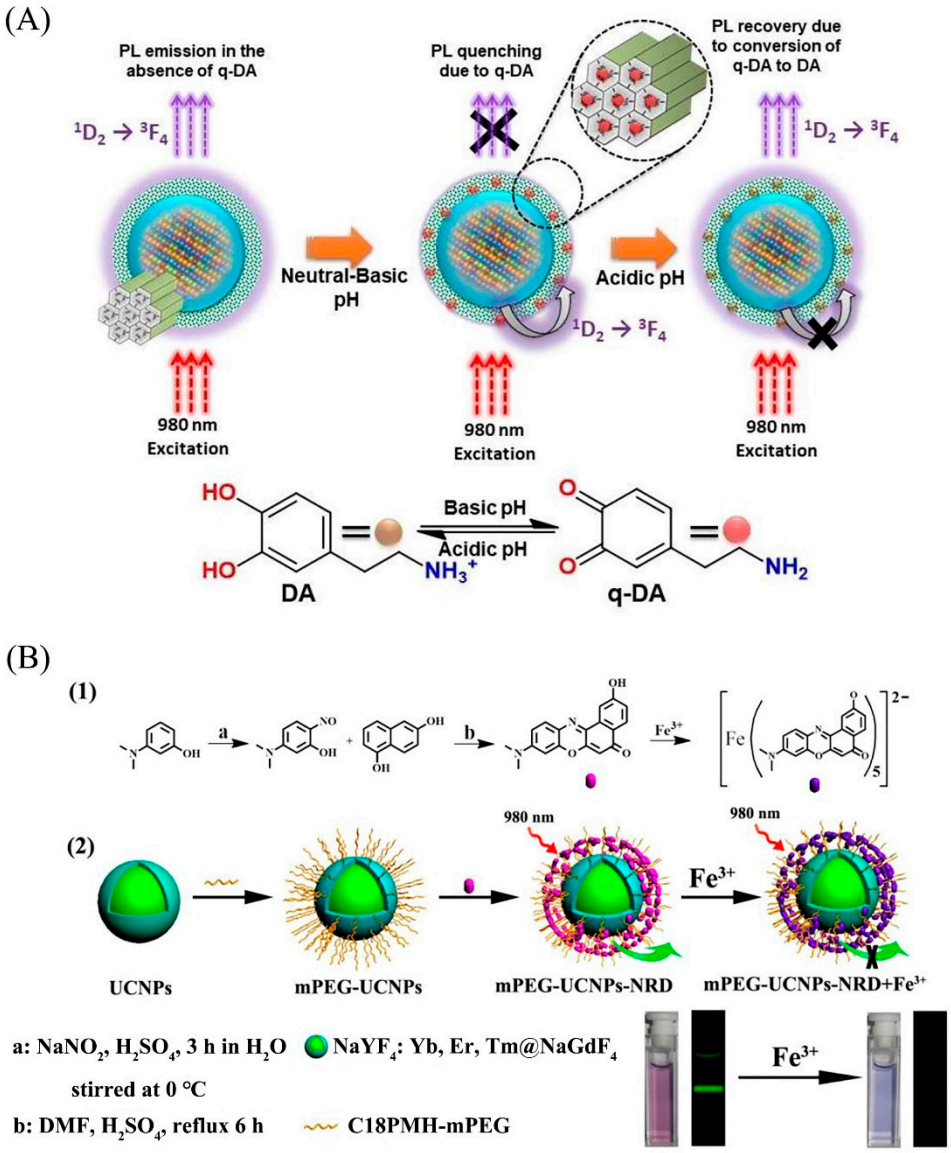

Figure 6. UCNPs in Analytical Application of Bioscience. (**A**) Concept of upconversion based nanoplatform (BCSU-MS) for dopamine (DA) and pH sensing. (**B**) (1) Illustration of the Synthesis of Nile Red Derivavite (NRD), (2) mPEG-UCNPs-NRD and Their Use for Detecting Fe^{3+} Based on Change in UCL Emission. Reprinted with permission from [127,153]. Copyright 2019, John Wiley and Sons and 2016, American Chemical Society.

H_2O_2 is one of the critical ROS molecules, which can provide very favorable evidence for significant diseases such as malignant tumor detection in vivo. Chen et al. [162] used an enzymatically controlled amplification strategy of circulating signals and designs colorimeter chains with acetylcholinesterase involved in forming H_2O_2 and Fenton reactions to detect H_2O_2 and glucose lactic and uric acid. This process can detect a variety of small molecules in vivo while analyzing and detecting H_2O_2, but the whole process for detecting H_2O_2 is a little complicated. Singh et al. [163] synthesized an UCNPs embedded organometallic complex HNPs, $NaYF_4$: Tm^{3+}/Yb^{3+}-Eu $(TTA)_3$Phen (ETP), which has great sensitivity to H_2O_2 and can be used many times without losing sensitivity. However, this framework may be more toxic to organisms. Wang et al. [164] designed a FRET system consists of an energy donor, a novel Nd^{3+}-sensitized UCNPs and the energy receptor dicyanomethylene-4H-pyran (DCM)-H_2O_2; utilizing the ratiometric fluorescence probe, the UCNPs luminescence (540 nm/660 nm) signal could visualize the H_2O_2 level. Additionally,

the LOD was quantified to be 0.168 μmol L^{-1}. This structure cannot cause an internal heat effect.

4.4.3. The UCNPs Analysis of Hydrogen Sulfide in Biological Samples

Hydrogen sulfide (H_2S) is a gas signaling molecule used to monitor acute pancreatitis in organisms and colorectal cancer [165]. Chen et al. [166] designed a sensing platform consisting of $NaGdF_4$: Yb, Er@$NaGdF_4$: Yb, Nd and IR-783. The dye-sensitized UCNPs nanoprobe has a dual-function of enhancing upconversion luminescence efficiency and specific recognition of H_2S, and the detection limit is as low as 34.17 nmol L^{-1}. Wang et al. [167] proposed poly (acrylic acid)-modified UCNPs assembled with cationic near-infrared cyanine chromophores (Cy_7-Cl) to detect H_2S in living cells and zebrafish, which can increase fluorescence of Cy_7-UCNPs, and completed the imaging work in vivo. Liu et al. [168] took Prussian Blue (PB) as the responder of H_2S, adding UCNPs performed by 5-nanometer lead envelopes. Employing the thickness of the lead envelope to detect H_2S in the serum range, the deficiency of Wang et al. [167] organic dye with specific toxicity was improved during imaging and detection. It can not only possess remarkable H_2S detection capacity, the LOD is 50 nmol L^{-1}, but was also feasible for H_2S elimination by UC-PB, reducing acute pancreatitis-associated lung injury and thus having excellent therapeutic potential as a drug.

4.5. Others

Glucose is the energy source of living cells and the intermediate product of metabolism in the body, and the content of glucose in the body is the data source for the diagnosis of diabetes. This is because glucose oxidase catalyzes glucose to produce gluconate hydrogen peroxide, which is associated with hydrogen peroxide usually during glucose analysis. Chen et al. [162] made use of this principle coupled with hydrogen peroxide, which catalyzes the conversion of ferrous to trivalent iron, and the trivalent ferric acid complex covers the converted fluorescence to obtain the analysis of glucose content. The experimental results are available, and the LOD can reach 2.3 μmol L^{-1}. UCNPs can superiorly reflect the advantage of removing background fluorescence in detecting tiny molecule organisms such as urea. Long et al. [91] utilized IFE effective between oxidizing o-phenylenediamine and $NaYF_4$: Yb^{3+}, Tm^{3+}, the low detection limit of uric acid is 6.7 μmol L^{-1}. While this complex procedure contains two oxidation processes, Zhou et al. [169] simplified the experiment by the process of adding Fe^{2+} to the hydroxyl radical reaction product of the oxidation reaction of uric acid. Furthermore, the detection limit is also much lower than before, as low as 1.90×10^{-3} μmol L^{-1}.

The mutagenic effects of drug residues on the hormonal action of organisms and bacterial resistance pose a continuous threat to the health of organisms. Furthermore, it has been a matter of immediate concern to medical experts in recent years. The determination of content of synthetic drug molecules in biological fluids has great significance in analytical biochemistry, clinical medical diagnosis, and local analysis or monitoring. The use of UCNPs for synthetic drug molecules sensing has attracted extensive interest because of their outstanding properties. The fluorescence of lanthanum (III) complex, produced by LRET from core–shell UCNPs, is sensitive to drug molecules. Hu et al. [58] utilized Yb^{3+}-Yb^{3+} energy migration was doping in $NaGdF_4$: Yb^{3+}, Er^{3+}@$NaYF_4$: Yb^{3+} can enhance luminescence intensity, when adding doxorubicin to the solution, doxorubicin can quench UCNPs by LRET. Additionally, the doxorubicin concentration of 0.005 μg g^{-1} in the mice can be successfully detected through the upconversion fluorescent probe. According to a similar principle, Mo et al. [170] prepared $NaYF_4$: Yb^{3+}, Er^{3+}, Nd^{3+}@$NaYF_4$: Nd^{3+} and successfully detected epirubicin, the LOD is 0.05 μmol L^{-1}.

Alprenolol is a drug for hypertension, while on the other hand, it has been designated a forbidden drug by the International Olympic Committee, because of its improper use related to controlling physical activity to minimize the heart rate, coronary blood flow, etc. Thus, Lee et al. [171] designed amphiphilic functional UCNPs which are ultra-highly selec-

tive for alprenolol. The electrostatic interaction of conjugated polythiophene functionalized $NaLuF_4$: Yb, Er with alprenolol resulted in specific recognition in human urine and serum with detection limits as low as 0.22 nmol L^{-1}.

The fluorescence properties, nice biocompatibility, and low background fluorescence of UCNPs can be used to monitor nutrients in crops and provide reference information for economic decisions of nutrient management. Guist et al. [172] used UCNPs ($NaYF_4$: Er^{3+}, Yb^{3+}) and Graphene Oxide to detect Zn deficiency in crops. At the time, smartphone color recognition had been successfully applied in this technology, which can quickly analyze Zn deficiency in barley or other crops. While the presence of a certain amount of UCNPs in organisms is also associated with specific toxicity, Modlitbová et al. [173] studied radish (Raphanus sativus L.) and common duckweed (Lemna minor L.) as adsorbed water-soluble UCNPs, as well as the toxicity, and bioaccumulation in these plants of UCNPs. Additionally, the length of the root per plant and the length of the hypocotyl per plant after 72 h exposure were chosen as toxicity endpoints, whereby 100 mg mL^{-1} of UCNPs/SiO_2-COOH was highly toxic.

On the other side, Popov, etc. [174] used fluorescence signals of the UCNPs in zebrafish and shrimps to quantitatively evaluate the temperature and pH of aquatic organisms' living environment in real time to determine the change in stress felt by organisms with the change in environment.

5. UCNPs in Analytical Application of Food and Medical Science

5.1. Analysis of Food Samples

Analysis of food sensing applications using UCNPs probes depends on several factors, including fluorescence, detection platform, and detection method. To achieve a specific and selective detection, UCNPs are functionalized with biological and chemical elements for target recognitions via typical antigen–antibody pairing, hybridization between complementary base pairs of nucleic acid, ionic interactions, etc. This chapter introduces the application of UCNPs in food analysis (milk, eggs, fruits, meat, drinking water), including residues of toxic and harmful substances, qualitative and quantitative analysis of harmful substances in food for humans, and the analytical application of enzymes and other active ingredients and summarizes the analytical profits in Table 6.

Food safety has always been an important issue related to human life safety, and the detection results of toxic and harmful substances residues in the diet are always an essential basis for food safety. After many experimental analyses on converting organophosphorus pesticides, nicotine pesticides, and other analytical applications, many researchers have obtained many research results. Organophosphorus pesticides (OPs) are widely used in agriculture because of their low persistence under natural conditions, easy synthesis, low cost, and high effectiveness for insect eradication. At the same time, they are neurotoxic due to their inhibition of acetylcholinesterase (AChE) in the central and peripheral nervous systems. Glyphosate is one of the OPs, Liu et al. [90] developed a colorimetric and fluorometric method based on a system composed of poly-ethylenimine-capped $NaGdF_4$: Yb, Er, copper (II) ions, hydrogen peroxide, and 3,3′,5,5′-tetramethylbenzidine. The UCNPs fluorescence of UCNPs can be quenched owing to the strong coordination between poly-ethylenimine and Cu (II) with the presence of glyphosate. So, it has good specificity. Fenitrothion [O, O-dimethyl O-(4-nitro-m-tolyl) phosphorothioate is also a broad-spectrum organophosphorus insecticide. The study of Yu et al. [175] was based on one immunochromatographic strip to detect 2,4-dichlorophenxyacetic acid and fenitrothion, utilizing specific recognition of anti-2,4-dichilorophenoxyactice acid immunoglobulin G (2,4-D-IgG) and rabbit anti-fenitrothion IgG combined with UCNPs medium to implement fluorescence detection. This method can realize real-time detection, which is easy to operate, while the preparation of rabbit antibodies remains to be commercialized.

Table 6. Application of UCNPs platform in food science.

Target		Samples	Platform	Characteristic	Linear Detection Range (ng mL^{-1})	LOD (ng mL^{-1})	Recovery (%)	RSD (%) (n=3)	Ref.
Organophosphorus pesticides	Chlorpyrifos	Apples, cucumbers	$NaYF_4$: Yb, Er-ChOx-Fe^{2+}	Accurate identification of chlorpyrifos through double-enzymes	20–2000	6.7	89.5–97.1%	–	[176]
	Malathion	Tap water, matcha	$NaYF_4$: Yb, Er-AuNPs	PDDA aptamer can specifically recognize malathion	3.3036–330.36	0.47	99–105.25 90–111.75	–	[177]
	Parathion-nmet-hyl, monocrotophos, dimethoate	Apples, cucumber, capsicum	$NaYF_4$: Yb, Er–AuNPs–AChE-acetylthiocholine (ATC)	Ensure AuNPs does not aggregate in the presence of pesticides and resulting in high efficiency of FRET	0.002–0.2	6.7×10^{-4} 0.023 0.067	96.67–110.00	4.78–8.43	[178]
	Glyphosate	Instant tea	$NaGdF_4$: Yb, Er-Cu^{2+}-H_2O_2-TMB	Fluorescence of $NaGdF_4$: Yb, Er at 660 nm increases linearly to form colorimetric assay	250–1.25×10^5	9.8	96.4–100.74	0.56–2.91	[90]
	Fenitrothion	–	Immunochromatographic strip consists of $NaYF_4$: Yb, Er-2, 4-D-IgG-fenitrothion-IgG	Portable sensors are prepared with unquestionable specificity	–	5	–	–	[175]
Neonicotinoid insecticides	Chlorpyrifos	Balloonflower angelica	$NaYF_4$: Yb, Tm-DA	Dopamine quinone quench FL of UCNPs through PEI and chlorpyrifos prevent oxidation of DA which recover UCNPs FL	1.0–10^3	0.38	95.4–120.0	5.3–8.5	[72]
	Diazinon	Apples	$NaGdF_4$: Yb, Tm-Cu^{2+}/AChE	Based on an (AChE) modulated fluorescence "off−on−off" strategy	0.1–50	0.05 ng mL^{-1}	93.2–102.1	5.7–8.3	[179]
	Diazinon	Tea, apples	$NaYF_4$: Yb, Er/Graphene Oxide	π-π interaction between UCNPs and GO	0.05–500	0.023	86.06–104.92 86.03–95.87	3.43–4.85	[180]
	Imidacloprid	Water, Chinese cabbage, honey	$NaYF_4$: Yb, Er/AuNPs	Dual signal of immunofluorescence improves the sensitivity and selectivity of imidacloprid.	1.39–335.81	0.79	78.1–97.9	3.4–11.2	[181]
	Acetamiprid	Paddy water, pears	$NaYF_4$: Yb, Er/cDNA-MNPs/aptamer	They label base complementary DNA, amine-functionalized UCNPs combine with negatively-charged DNA through electrostatic interaction	0.89–114.18	650	78.2–103.5	2.6–10.9	[182]
		Apples, strawberry	$NaYF_4$: Yb, Er@molecularly imprinted polymer (MIP)	Quenching UCNPs emission peak at 542nm and specific recognition of MIP	20–800	8.3	89.6–97.9	1.6–2.9	[183]
	Deltamethrin	Grape, cabbage	$NaYF_4$: Yb, Er@MNPs@MIPs	Difunctional materials ensure a high degree selectivity of deltamethrin and separation	10^3 –10^6	0.749	95.6–02% 91.8–05%	2.97–4.07 2.42–5.20	[184]
Pyrethroids pesticides	Fenpropathrin, Cypermethrin, fenvalerate	Cucumber, cabbage, apples and pears	$NaYF_4$@$NaYF_4$: Yb, Er@$NaYF_4$/aminoated polystyrene magnetic microspheres-antigen	Devices for detecting multiple targets and miniaturized readout devices	–	0.01 0.015 0.011	83.4–97.8	–	[185]

Table 6. *Cont.*

Target		Samples	Platform	Characteristic	Linear Detection Range (ng mL^{-1})	LOD (ng mL^{-1})	Recovery (%)	RSD (%) (n=3)	Ref.
Carbamate pesticide	Carbaryl	Tea	$NaErF_4$: Tm^{3+}@$NaYF_4$/polydopamine embedded sodium alginate hydrogel	UCNPS immobilized-sodium alginate hydrogel system realizes the true sense of field detectable	0.5–200	0.5	90.51–105.33	2.28–4.46	[186]
Benz-fungicide imidazole	CBZ	Apples, cucumber, matcha powder	$NaGdF_4$: Yb, Er/MnO_2	The aptamer can self-assemble on the MnO_2 nanosheet surface to quenching UCNPs FL	0.1–5000	0.05	93.84–96.62 90.14–93.96 93.80–109.4	2.02–4.39 2.90–4.30 1.87–3.51	[187]
Rhodamine B		Opaque fishes	$NaYF_4$: Yb, Er	Opaque fishes not absorb RB and it will be quenching UCNPs FL through FRET	–	–	–	–	[188]
Norfloxacin		Milk	$NaYF_4$: Yb, Er	Comparing analysis results of NOR strips, QD FICS and UCNPs FICS and LOD of UCNPs is lowest.	–	0.5	–	–	[189]
	Kanamycin	Milk, tap water	$NaGd/YF_4$: Yb, Er-aptamer/BHQ_3-cDNA	Kanamycin disrupts the FRET between BHQ_3 and UCNPs by pairing with aptamer	24.2–2.42×10^4	9.15	87–109.6 95.6–108.8	–	[190]
	Gallic acid	Green tea, orange juice	$NaErF_4$: Tm@SiO_2@ZIF-8/TMB	The emission spectrum of $NaErF_4$: Tm@SiO_2@ZIF-8 has overlap with the absorption spectra of oxTMB	0–5103.6	59.542	98.4–105	0.6–2.3	[136]
	Cu^{2+}	–	$NaYF_4$@$NaYF_4$: Er, Yb@$NaYF_4$/rhodamine B hydrazide (RBH)	The distance between $Er^{3+}$and RHB can enhance FL of UCNPs to improve signal sensitivity	–	–	—	-	[191]
Metal ion	Pb^{2+}	Tea	$NaYF_4$: Gd, Yb, Ho/MNPs-AuNPs	Addition base complementary recognition to electrostatic interaction to construct FRET sensing platform	2.05–114.8	0.4674	101.6–107.0	0.8–2.1	[57]
	Hg^{2+}	Green tea	$NaYF_4$: Yb, Er@$NaYF_4$/AuNPs-cysteine	Fluorescence turns off-on-off to detect Hg^{2+}	0.48–480	1.08	93–102	1.57–2.06	[192]
		Ribbon fish	T-$NaYF_4$: Yb, Tm	UCNP-T-Hg^{2+}-T-UCNP reticular architecture on the surface of the electrode can accumulation of UCNP	2.01×10^{-3}–0.201	8.04×10^{-5}	–	–	[193]
IAcid ion	F	Milk	$NaYF_4$: Yb, Er, Tm/curcumin	The specific recognition of curcumin with fluoride ions caused the shift in the UCNPs characteristic peak	475–3.8×10^3 95–2.18×10^4	475	79.58–134.02%	0.94–22.11	[194]
	HSO_3^-	Sugar	$NaYF_4$: Yb, Er@$NaYF_4$/cyanine dye	$NOBF_4$ functionalized UCNPs to electrostatic adsorption with cyanine dyes	81–9720	5.67	99.9–103.8	–	[195]

Neonicotinoid insecticides have persistence and high solubility, and they can affect the nervous system. Imidacloprid is a type of neonicotinoid insecticide that attracts numer-

ous researchers to analyze its environmental residual. Si et al. [144] set a homogeneous immunoassay, and the analysis signal is derived from IFE between UCNPs and AuNPs. UCNPs are coupled to the antibody against imidacloprid, and AuNPs are used to label the antigen of imidacloprid. The competitive immunoreaction occurred between imidacloprid and antigen-AuNPs binding to antibody-UCNPs. If this method can be applied to polystyrene micro-well plates, the corresponding microplate readers should be developed to enable high-throughput screening. Sun et al. [145] successfully detected acetamiprid in rice, apple, pear, wheat, and cucumber using an acetamiprid aptamer-modified magnetic nanoparticle UCNPs fluorescent probe, and the detection limit is 0.65 μg L^{-1}. Yu et al. [146] studied that because antibodies are susceptible to interference by organic solvents and other components in food, and the chemical stability of molecular imprinting is well known. They studied UCNPs@SiO2-MIP to detect acetamiprid in apples and strawberries, and the LOD is 8.3 ng mL^{-1}.

In this review, the application of UCNPs in the detection of organic reagents in food in recent years is introduced in chronological order. Hu et al. [188] prepared polyethylene glycol hybrid ligand $NaLuF_4$: Yb^{3+} and Er^{3+}, and determined Rhodenine B and sodium fluorescein content in living opaque fish according to the position and intensity of its emission peak and luminescence resonant energy transfer between the fluorescent materials. Rong et al. [196] prepared a sensing platform consists of PEI-$NaYF_4$: Yb, Er and GSH coupled with RBD to detect acrylamide. This study's application can make food safety analysis faster and simpler. Wang et al. [197] determined the quality of red wine by analyzing the tannic acid content in red wine. They designed three different conjugated structures UCNPs: UCNPs@GDN, UCNPs@SO_3H, UCNPs@$PO(OH)_2$ were used to verify the efficiency of electron transfer between the material and tannic acid, and the results after transfer, respectively, through single, pairwise mixing and three mixed experiments to judge tannic acid. The content of tannic acid was also determined. In addition, the array calculation method successfully identified a variety of red wines. Hu et al. [189] made an immune chromatography test paper tag (antibody colloidal gold-quantum dots-UCNPs) for the visual judgment of milk, with different concentrations of norfloxacin, in the analysis of the sensitivity of a variety of fluorescent materials added, which can also compare quantum dots and the conversion of functional strength. The experiments show that quantum dots are the most sensitive of norfloxacin, while the UCNPs provide the most accurate analysis results in the milk. In order to detect heterocyclic aromatic amine carcinogens in fried meat products, Huang et al. [198] used $NaYF_4$: Yb, Er grafted with anti-2-amino-3-methylimidazo [4, 5-f] quinoline (IQ) antibodies as fluorescent sensor through immunofluorescence sensing to detect IQ, and the LOD was as low as 7 ng L^{-1}.

Currently, UCNPs are being widely used to detect active components such as enzymes in organisms, which is a mighty popular application. However, it is difficult to detect the enzyme in food because detection becomes difficult with changes in the environment. Detection becomes difficult. del Barrio et al. [199] successfully detected glucose oxidase in fruit juice using near-infrared-excited Tm^{3+} and Yb^{3+} to prepare fluorohemiflurate and pyrene fluorescein-conjugated graphene oxide mixed and coated on glass casting. This material has upconversion properties which should be more widely used in many more studies.

Inorganic ion residues in food can lead to reduced immunity and imbalance in trace element levels, etc. Qualitative and quantitative analysis of metal ions and inorganic salts in food is also particularly important. Zhang et al. [191] planed a FRET system including $NaYF_4$@$NaYF_4$: Er^{3+}/Yb^{3+}@$NaYF_4$, which exhibit characteristic green emissions UCNPs and rhodamine B hydrazide (RBH), which is nonfluorescent. Adding Cu^{2+} to this system, a luminescence decrease in the nanoparticles occurs due to the energy transfer from UCNPs to RBH. Moreover, the structure design is in favor of improving sensitivity for Cu^{2+} detection and enhancing UCL detection signal. Chen et al. [57] used aptamer and FRET immunological recognition between $NaYF_4$: Gd, Yb, Ho, and magnetic Fe_3O_4-modified (MNPs) GNPs, which generates a specific response to Pb^{2+} for dual recognition.

It is sensitive to obtaining lead ions' content in tea, and the detection limit is as low as 5.7 nmol L^{-1}.

Fluoride ion is helpful for dental care and treatment of osteoporosis, while intaking excessively has negative active impacts on human health. Liu et al. [194] utilized IFE between amino-modified Yb^{3+}, Er^{3+}, Tm^{3+}, co-doped $NaYF_4$, and curcumin-F^- complex. The addition of F^- could cause a bathochromic shift in the maximum UV absorption peak of curcumin occurs and leads to the IFE-quenched fluorescence of UCNPs the large absorption bathochromic shift. Additionally, this results in a color change, which can be observed as well. This sensor has a fabulous response to F^- and has been successfully applied to milk products. It has an outstanding application prospect.

5.2. Analysis of Medical Sample

Synthetic drug molecules have played a decisive role in the history of human health. However, the residues of drugs in treating diseases and the number of residues should be of immediate concern. The application of the UCNPs in drug analysis has also been part of the research. Of course, if this fluorescence sensing platform can be combined with the real-time monitoring of people's lives during the administration of drugs, it will be a future direction for the development of medicine and fluorescence analysis.

The fluorescence of lanthanum (III) complexes produced by LRET from core–shell UCNPs is sensitive to drug molecules. Zhang et al. [65] imported SYBR Green-I as an energy donor to establish an LRET system with UCNPs to detect oxytetracycline. On the one hand, SYBR Green-I shows very week fluorescence unbinding with dsDNA. On the other hand, oxytetracycline stops combining with dsDNA and SYBR Green-I, then recovering UCNPs luminescence. This sensor is susceptible to LOD as low as 0.054 ng mL^{-1} (Figure 7A).

UCNPs are used to combine with precious metals such as gold and silver nanoparticles using Surface-enhanced Raman scattering (SERS) technology. At the same time, the SERS enhancement degree has extreme dependence on the excitation wavelength, and long-time exposure to the object under test under the irradiation of ultraviolet, visible laser power loss will have a certain degree. The near-infrared excitation of UCNPs will help it. Ma et al. [200] made $NaYF_4$: Yb, Er@SiO_2@Ag, which significantly improved the Raman enhancement ability of silver nanoparticles. Additionally, it was used to detect methylamphetamine successfully. It provides a new method for drug analysis.

In order to use quick and convenient fluorescence spectroscopy to analyze drugs, molecularly imprinted polymers (MIPs) are always used in combination with up-conversion nanoparticles with low background fluorescence due to their excellent selectivity. Tang et al. [60] synthesized layer-by-layer compounds of MIP and Fe_3O_4 nanoparticles on $NaYF_4$: Yb^{3+}, Er^{3+}particles (MUCPs@MIP). They tested multiple drugs by using different quinolones as templates. Moreover, core–shell MIPs are designed to overcome some drawbacks such as the nonuniform distribution of binding sites, uncompleted removal of template or leakage, slow mass transfer, irregular morphology, etc. They are also designed to enhance recognition efficiency (Figure 7B).

Immunofluorescence analysis is also a commonly used analytical method, Zhang et al. [201] designed a lateral flow immunochromatographic and UCNPs to detect triamcinolone acetonide (TCA) cosmetics. Immunochromatography combined with fluorescence spectrum essentially solves the problems of narrow linear range, low sensitivity, and rough quantitative results. Additionally, the LOD for TCA in a cosmetic sample is 20 μg kg^{-1}.

Drug anti-counterfeiting is an innovation in the application of UCNPs in medical science; a smart phone identification technology based on an upconversion fluorescent 3D quick response code for tracking and anti-counterfeiting of a drug was developed by You et al. [73]. They were resolving some drawbacks in existing anti-counterfeit technology such as high cost, complex fabrication process, and sophisticated operation as well. Multilayer inkjet printing and segmentation will also increase the amount of information

stored per unit area. QR contains drug information also. Therefore, an upconversion fluorescent-based 3D QR code is promising as a powerful tool for drug anti-counterfeiting.

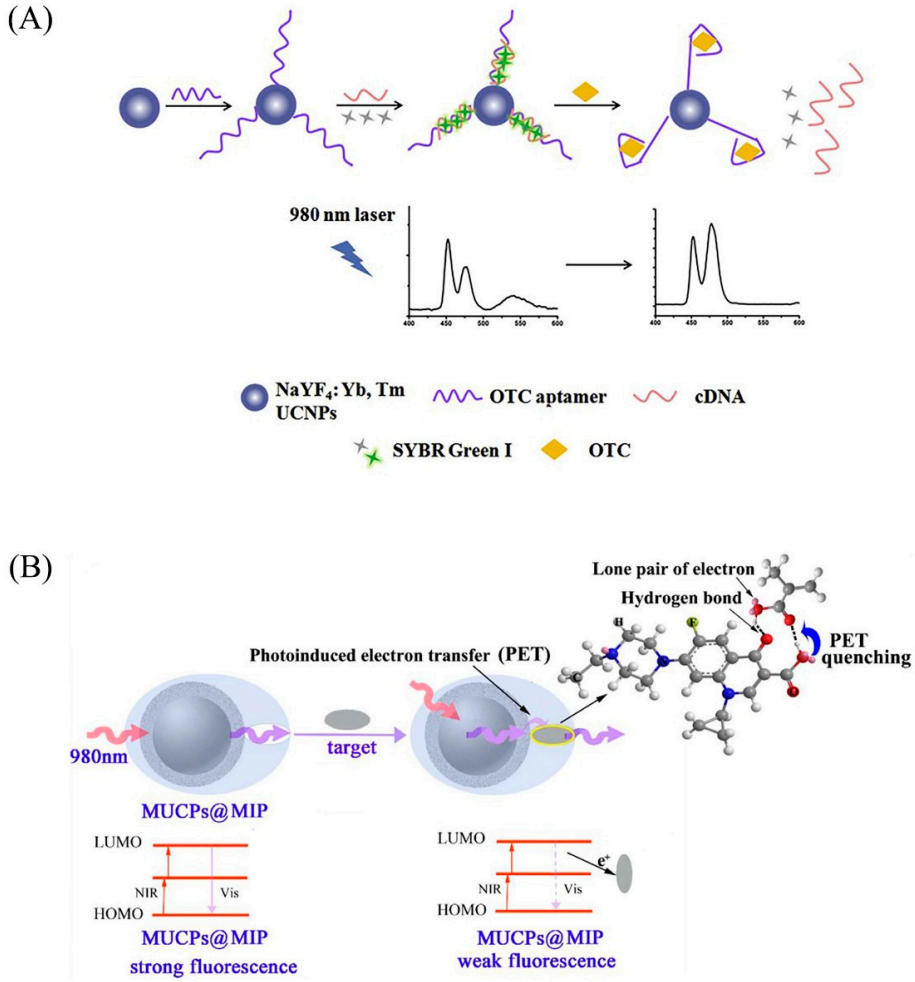

Figure 7. (**A**) Schematic illustration of the sensitive aptasensor for oxytetracycline based on upconversion luminescence resonance energy transfer. (**B**) Schematic diagram of quinolones fluorescence quenching the UCNPs mechanism. Reprinted with permission from [60,65]. Copyright 2015 and 2018, Elsevier.

6. Conclusions and Perspectives

Basing on the special fluorescent properties of the UCNPs, the progress of research on one synthesis and analysis application of the UCNPs was reported in this review. The applications of UCNPs probes for analytical detection in environmental science, bioscience, food science, and medical science were summarized.

The application of the UCNPs in the field of analysis had attracted the attention of more and more researchers. Additionally, future research will focus on how to better utilize the excellent properties of the UCNPs in anticipation of solving the applications that have emerged, such as its weak detection signal, weak specificity, low detection range, and it not being widely used for real-time detection problems:

I. Different testing environments set different conditions for researchers, affecting the performance of UCNPs applications. So, the improvement in the luminescence efficiency of UCNPs according to the different analytical environments is a question worthy of deep pondering.

II. Designing practical UCNPs analysis platforms for different target analytes remains one of the challenges of applied research: (i) Depending on the type of substance to be measured, such as inorganic ions, small organic molecules, biological macromolecules,

etc., the design of the UCNPs analysis platform with high matching to the properties of the substance to be measured to improve the selectivity is a challenge to be overcome in future integrated substance analysis. (ii) The study of easy functionalization of the UCNPs has already been applied in the field of analysis. In the following research to take more targeted functionalization of the UCNPs. According to the nature of the substances to be measured, the scope of application of the UCNPs in analytical chemistry becomes broader. Additionally, it will become another hot issue in the field of the UCNPs analysis in the future.

III. From the applicated materials, test methods, analysis conditions, test environment, and other aspects of the study on the impact of various factors on the test results, dedication to improving the efficiency of the analysis is also the future of the analysis process, thus requiring researchers to explore the direction of their efforts.

Based on the many desirable properties of the UCNPs mentioned in the paper and the wide range of applications of the UCNPs in the analytical field, they will essentially solve most of the challenging problems faced in today's applications as the research progresses.

Author Contributions: W.J. and J.Y. contributed equally to this work. Conceptualization, J.Y. and X.L.; writing—original draft preparation, W.J., J.Y. and X.L.; writing—review and editing, W.J., N.N. and L.C.; visualization, X.L. and F.H.; supervision, N.N. and L.C.; funding acquisition, F.H. and L.C. All authors have read and agreed to the published version of the manuscript.

Funding: This research was funded by Fundamental Research Funds for the Central Universities (2572022DJ01), 111 Project (B20088), Heilongjiang Touyan Innovation Team Program (Tree Genetics and Breeding Innovation Team), Key Laboratory of Superlight Materials and Surface Technology (Harbin Engineering University) and Natural Science Foundation of Heilongjiang Province (LH2002B002).

Institutional Review Board Statement: Not applicable.

Informed Consent Statement: Not applicable.

Data Availability Statement: Not applicable.

Conflicts of Interest: The authors declare no conflict of interest.

References

1. Wang, F.; Han, Y.; Lim, C.S.; Lu, Y.; Wang, J.; Xu, J.; Chen, H.; Zhang, C.; Hong, M.; Liu, X. Simultaneous phase and size control of upconversion nanocrystals through lanthanide doping. *Nature* **2010**, *463*, 1061–1065. [CrossRef]
2. Chen, G.; Qiu, H.; Prasad, P.N.; Chen, X. Upconversion Nanoparticles: Design, Nanochemistry, and Applications in Theranostics. *Chem. Rev.* **2014**, *114*, 5161–5214. [CrossRef]
3. Xu, J.; Gulzar, A.; Yang, D.; Gai, S.; He, F.; Yang, P. Tumor self-responsive upconversion nanomedicines for theranostic applications. *Nanoscale* **2019**, *11*, 17535–17556. [CrossRef] [PubMed]
4. Tan, G.-R.; Wang, M.; Hsu, C.-Y.; Chen, N.; Zhang, Y. Small Upconverting Fluorescent Nanoparticles for Biosensing and Bioimaging. *Adv. Opt. Mater.* **2016**, *4*, 984–997. [CrossRef]
5. Gulzar, A.; Xu, J.; Yang, P.; He, F.; Xu, L. Upconversion processes: Versatile biological applications and biosafety. *Nanoscale* **2017**, *9*, 12248–12282. [CrossRef]
6. Wang, F.; Liu, X. Recent advances in the chemistry of lanthanide-doped upconversion nanocrystals. *Chem. Soc. Rev.* **2009**, *38*, 976–989. [CrossRef] [PubMed]
7. Wang, F.; Liu, X. Upconversion Multicolor Fine-Tuning: Visible to Near-Infrared Emission from Lanthanide-Doped $NaYF_4$ Nanoparticles. *J. Am. Chem. Soc.* **2008**, *130*, 5642–5643. [CrossRef]
8. Tüzen, M. Determination of heavy metals in soil, mushroom and plant samples by atomic absorption spectrometry. *Microchem. J.* **2003**, *74*, 289–297. [CrossRef]
9. Jahromi, E.Z.; Bidari, A.; Assadi, Y.; Hosseini, M.R.M.; Jamali, M.R. Dispersive liquid–liquid microextraction combined with graphite furnace atomic absorption spectrometry: Ultra trace determination of cadmium in water samples. *Anal. Chim. Acta* **2007**, *585*, 305–311. [CrossRef] [PubMed]
10. Batista, É.A.; Silva, G.; Sgobbi, L.; Machado, F.; Macedo, I.; Moreno, E.; Neto, J.; Scalize, P.; Gil, E. Enzymatic Electroanalytical Biosensor Based on *Maramiellus colocasiae* Fungus for Detection of Phytomarkers in Infusions and Green Tea Kombucha. *Biosensors* **2021**, *11*, 91. [CrossRef] [PubMed]
11. Zhang, B.; Hou, X.; Zhen, C.; Wang, A.X. Sub-Part-Per-Billion Level Sensing of Fentanyl Residues from Wastewater Using Portable Surface-Enhanced Raman Scattering Sensing. *Biosensors* **2021**, *11*, 370. [CrossRef] [PubMed]

12. Majchrzak, T.; Wojnowski, W.; Lubinska-Szczygeł, M.; Różańska, A.; Namieśnik, J.; Dymerski, T. PTR-MS and GC-MS as complementary techniques for analysis of volatiles: A tutorial review. *Anal. Chim. Acta* **2018**, *1035*, 56. [CrossRef]
13. Lv, G.; Liu, S.; Liu, M.; Liao, L.; Wu, L.; Mei, L.; Li, Z.; Pan, C. Detection and quantification of phenol in liquid and gas phases using a clay/dye composite. *J. Ind. Eng. Chem.* **2018**, *62*, 284–290. [CrossRef]
14. Han, C.; Li, H. Host-molecule-coated quantum dots as fluorescent sensors. *Anal. Bioanal. Chem.* **2009**, *397*, 1437–1444. [CrossRef] [PubMed]
15. Wang, B.; Liu, B.; Yan, Y.; Tang, K.; Ding, C.-F. Binary magnetic metal-organic frameworks composites: A promising affinity probe for highly selective and rapid enrichment of mono- and multi-phosphopeptides. *Mikrochim. Acta* **2019**, *186*, 832. [CrossRef]
16. Haase, M.; Schäfer, H. Upconverting Nanoparticles. *Angew. Chem. Int. Ed.* **2011**, *50*, 5808–5829. [CrossRef]
17. Boyer, J.-C.; Vetrone, F.; Cuccia, L.A.; Capobianco, J.A. Synthesis of Colloidal Upconverting $NaYF_4$ Nanocrystals Doped with Er^{3+}, Yb^{3+} and Tm^{3+}, Yb^{3+} via Thermal Decomposition of Lanthanide Trifluoroacetate Precursors. *J. Am. Chem. Soc.* **2006**, *128*, 7444–7445. [CrossRef] [PubMed]
18. Vetrone, F.; Naccache, R.; Mahalingam, V.; Morgan, C.G.; Capobianco, J.A. The Active-Core/Active-Shell Approach: A Strategy to Enhance the Upconversion Luminescence in Lanthanide-Doped Nanoparticles. *Adv. Funct. Mater.* **2009**, *19*, 2924–2929. [CrossRef]
19. Song, Y.; Gong, G.; Du, J.; Xie, S.; Ouyang, M.; Feng, Y.; Xu, J.; Xu, L. Synthesis and Inkjet Printing of $NaYF_4$:Ln^{3+}@$NaYF_4$ Core–Shell Nanoparticles with Enhanced Upconversion Fluorescence for Anti-Counterfeiting Applications. *J. Nanosci. Nanotechnol.* **2020**, *20*, 1511–1519. [CrossRef]
20. Yi, G.S.; Chow, G.M. Synthesis of Hexagonal-Phase NaYF4:Yb,Er and NaYF4:Yb,Tm Nanocrystals with Efficient Up-Conversion Fluorescence. *Adv. Funct. Mater.* **2006**, *16*, 2324–2329. [CrossRef]
21. Li, C.; Quan, Z.; Yang, J.; Yang, A.P.; Lin, J. Highly Uniform and Monodisperse β-$NaYF_4$:Ln^{3+} (Ln = Eu, Tb, Yb/Er, and Yb/Tm) Hexagonal Microprism Crystals: Hydrothermal Synthesis and Luminescent Properties. *Inorg. Chem.* **2007**, *46*, 6329–6337. [CrossRef]
22. Chen, Z.; Chen, H.; Hu, H.; Yu, M.; Li, F.; Zhang, Q.; Zhou, Z.; Yi, T.; Huang, C. Versatile Synthesis Strategy for Carboxylic Acid−functionalized Upconverting Nanophosphors as Biological Labels. *J. Am. Chem. Soc.* **2008**, *130*, 3023–3029. [CrossRef] [PubMed]
23. Qiang, Q.; Wang, Y. Enhanced optical temperature sensing and upconversion emissions based on the Mn^{2+} codoped $NaGdF_4$:Yb^{3+},Ho^{3+} nanophosphor. *New J. Chem.* **2018**, *43*, 5011–5019. [CrossRef]
24. Liangab, S.; Sunac, C.; Yangc, P.; Ping'Anmaab, P.; Huanga, S.; Chengab, Z.; Yubd, X.; Linab, J. Core-shell structured upconversion nanocrystal-dendrimer composite as a carrier for mitochondria targeting and catalase enhanced anti-cancer photodynamic therapy. *Biomaterials* **2020**, *240*, 119850. [CrossRef] [PubMed]
25. Shao, H.; Xu, D.; Ding, Y.; Hong, X.; Liu, Y. An "off-on" colorimetric and fluorometric assay for Cu(II) based on the use of NaYF4:Yb(III),Er(III) upconversion nanoparticles functionalized with branched polyethylenimine. *Mikrochim. Acta* **2018**, *185*, 211. [CrossRef] [PubMed]
26. Wei, T.; Yang, F.; Jing, Q.; Zhao, C.; Wang, M.; Du, M.; Guo, Y.; Zhou, Q.; Li, Z. Optical multi-functionalities of Er3+- and Yb3+-sensitized strontium bismuth titanate nanoparticles. *J. Alloy. Compd.* **2019**, *801*, 100. [CrossRef]
27. Su, S.; Mo, Z.; Tan, G.; Wen, H.; Chen, X.; Hakeem, D.A. PAA Modified Upconversion Nanoparticles for Highly Selective and Sensitive Detection of Cu2+ Ions. *Front. Chem.* **2021**, *8*, 619764. [CrossRef]
28. Liu, J.; Bu, W.; Zhang, S.; Chen, F.; Xing, H.; Pan, L.; Zhou, L.; Peng, W.; Shi, J. Controlled Synthesis of Uniform and Monodisperse Upconversion Core/Mesoporous Silica Shell Nanocomposites for Bimodal Imaging. *Chem. A Eur. J.* **2012**, *18*, 2335–2341. [CrossRef]
29. Wang, C.; Xu, L.; Xu, J.; Yang, D.; Liu, B.; Gai, S.; He, F.; Yang, P. Multimodal imaging and photothermal therapy were simultaneously achieved in the core–shell UCNR structure by using single near-infrared light. *Dalton Trans.* **2017**, *46*, 12147–12157. [CrossRef]
30. Zhao, J.; Sun, Y.; Kong, X.; Tian, L.; Wang, Y.; Tu, L.; Zhao, J.; Zhang, H. Controlled Synthesis, Formation Mechanism, and Great Enhancement of Red Upconversion Luminescence of $NaYF_4$:Yb^{3+}, Er^{3+} Nanocrystals/Submicroplates at Low Doping Level. *J. Phys. Chem. B* **2008**, *112*, 15666–15672. [CrossRef]
31. Li, H.; Liu, G.; Wang, J.; Dong, X.; Yu, W. Dual-mode, tunable color, enhanced upconversion luminescence and magnetism of multifunctional $BaGdF_5$:Ln^{3+} (Ln = Yb/Er/Eu) nanophosphors. *Phys. Chem. Chem. Phys.* **2016**, *18*, 21518–21526. [CrossRef] [PubMed]
32. Märkl, S.; Schroter, A.; Hirsch, T. Small and Bright Water-Protected Upconversion Nanoparticles with Long-Time Stability in Complex, Aqueous Media by Phospholipid Membrane Coating. *Nano Lett.* **2020**, *20*, 8620–8625. [CrossRef]
33. Lu, Y.; Wang, L.; Chen, H. Turn-on detection of MicroRNA155 based on simple UCNPs-DNA-AuNPs luminescence energy transfer probe and duplex-specific nuclease signal amplification. *Spectrochim. Acta Part A Mol. Biomol. Spectrosc.* **2019**, *223*, 117345. [CrossRef]
34. Johnson, N.J.J.; Sangeetha, N.M.; Boyer, J.-C.; van Veggel, F.C.J.M. Facile ligand-exchange with polyvinylpyrrolidone and subsequent silica coating of hydrophobic upconverting β-NaYF4:Yb3+/Er3+ nanoparticles. *Nanoscale* **2010**, *2*, 771–777. [CrossRef] [PubMed]
35. Hazra, C.; Ullah, S.; Correales, Y.E.S.; Caetano, L.G.; Ribeiro, S.J.L. Enhanced NIR-I emission from water-dispersible NIR-II dye-sensitized core/active shell upconverting nanoparticles. *J. Mater. Chem. C* **2018**, *6*, 4777–4785. [CrossRef]

36. Zhang, Q.; Wang, W.; Zhang, M.; Wu, F.; Zheng, T.; Sheng, B.; Liu, Y.; Shen, J.; Zhou, N.; Sun, Y. A theranostic nanocomposite with integrated black phosphorus nanosheet, Fe3O4@MnO2-doped upconversion nanoparticles and chlorin for simultaneous multimodal imaging, highly efficient photodynamic and photothermal therapy. *Chem. Eng. J.* **2020**, *391*, 123525. [CrossRef]
37. Wang, Q.-Q.; Hu, R.; Fang, Z.-Q.; Shi, G.; Zhang, S.; Zhang, M. A multifunctional upconversion nanoparticles probe for Cu2+ sensing and pattern recognition of biothiols. *Chin. Chem. Lett.* **2021**, *33*, 3782–3786. [CrossRef]
38. Zhang, F.; Wan, Y.; Yu, T.; Zhang, F.; Shi, Y.; Xie, S.; Li, Y.; Xu, L.; Tu, B.; Zhao, D. Uniform Nanostructured Arrays of Sodium Rare-Earth Fluorides for Highly Efficient Multicolor Upconversion Luminescence. *Angew. Chem. Int. Ed.* **2007**, *46*, 7976–7979. [CrossRef]
39. Bu, W.; Chen, Z.; Chen, F.; Shi, J. Oleic Acid/Oleylamine Cooperative-Controlled Crystallization Mechanism for Monodisperse Tetragonal Bipyramid NaLa(MoO_4)$_2$ Nanocrystals. *J. Phys. Chem. C* **2009**, *113*, 12176–12185. [CrossRef]
40. Liu, S.; De, G.; Xu, Y.; Wang, X.; Liu, Y.; Cheng, C.; Wang, J. Size, phase-controlled synthesis, the nucleation and growth mechanisms of NaYF4:Yb/Er nanocrystals. *J. Rare Earths* **2018**, *36*, 1060–1066. [CrossRef]
41. Lu, S.; Tu, D.; Li, X.; Li, R.; Chen, X. A facile "ship-in-a-bottle" approach to construct nanorattles based on upconverting lanthanide-doped fluorides. *Nano Res.* **2015**, *9*, 187–197. [CrossRef]
42. Na, H.; Woo, K.; Lim, K.; Jang, H.S. Rational morphology control of β-NaYF4:Yb,Er/Tm upconversion nanophosphors using a ligand, an additive, and lanthanide doping. *Nanoscale* **2013**, *5*, 4242–4251. [CrossRef]
43. Li, Z.; Zhang, Y. An efficient and user-friendly method for the synthesis of hexagonal-phase $NaYF_4$:Yb, Er/Tm nanocrystals with controllable shape and upconversion fluorescence. *Nanotechnology* **2008**, *19*, 345606. [CrossRef]
44. Ding, M.; Yin, S.; Chen, D.; Zhong, J.; Ni, Y.; Lu, C.; Xu, Z.; Ji, Z. Hexagonal NaYF4:Yb3+/Er3+ nano/micro-structures: Controlled hydrothermal synthesis and morphology-dependent upconversion luminescence. *Appl. Surf. Sci.* **2015**, *333*, 23–33. [CrossRef]
45. Li, S.; Ye, S.; Chen, X.; Liu, T.; Guo, Z.; Wang, D. OH− ions-controlled synthesis and upconversion luminescence properties of NaYF4:Yb3+,Er3+ nanocrystals via oleic acid-assisted hydrothermal process. *J. Rare Earths* **2017**, *35*, 753–760. [CrossRef]
46. Lin, H.; Xu, D.; Li, A.; Teng, D.; Yang, S.; Zhang, Y. Morphology evolution and pure red upconversion mechanism of β-NaLuF4 crystals. *Sci. Rep.* **2016**, *6*, 28051. [CrossRef]
47. Qiu, P.; Sun, R.; Gao, G.; Zhang, C.; Chen, B.; Yan, N.; Yin, T.; Liu, Y.; Zhang, J.; Yang, Y.; et al. An Anion-Induced Hydrothermal Oriented-Explosive Strategy for the Synthesis of Porous Upconversion Nanocrystals. *Theranostics* **2015**, *5*, 456–468. [CrossRef] [PubMed]
48. Bogdan, N.; Vetrone, F.; Ozin, G.A.; Capobianco, J.A. Synthesis of Ligand-Free Colloidally Stable Water Dispersible Brightly Luminescent Lanthanide-Doped Upconverting Nanoparticles. *Nano Lett.* **2011**, *11*, 835–840. [CrossRef]
49. Wang, M.; Abbineni, G.; Clevenger, A.; Mao, C.; Xu, S. Upconversion nanoparticles: Synthesis, surface modification and biological applications. *Nanomed. Nanotechnol. Biol. Med.* **2011**, *7*, 710–729. [CrossRef] [PubMed]
50. Li, Z.; Zhang, Y. Monodisperse Silica-Coated Polyvinylpyrrolidone/NaYF4 Nanocrystals with Multicolor Upconversion Fluorescence Emission. *Angew. Chem. Int. Ed.* **2006**, *45*, 7732–7735. [CrossRef] [PubMed]
51. Xu, M.; Yang, G.; Bi, H.; Xu, J.; Dong, S.; Jia, T.; Wang, Z.; Zhao, R.; Sun, Q.; Gai, S.; et al. An intelligent nanoplatform for imaging-guided photodynamic/photothermal/chemo-therapy based on upconversion nanoparticles and CuS integrated black phosphorus. *Chem. Eng. J.* **2020**, *382*, 122822. [CrossRef]
52. He, B.; Zhou, L. Efficient tailoring of the surface of upconversion nanoparticles via surface-initiated cationic ring-opening polymerization. *RSC Adv.* **2015**, *5*, 97764–97772. [CrossRef]
53. Sun, L.; Wang, T.; Sun, Y.; Li, Z.; Song, H.; Zhang, B.; Zhou, G.; Zhou, H.; Hu, J. Fluorescence resonance energy transfer between NH_2–$NaYF_4$:Yb,Er/$NaYF_4$@SiO_2 upconversion nanoparticles and gold nanoparticles for the detection of glutathione and cadmium ions. *Talanta* **2019**, *207*, 120294. [CrossRef]
54. Shi, H.; Nie, Q.; Yang, M.; Wang, C.; Liu, E.; Ji, Z.; Fan, J. A ratiometric fluorescence probe for melamine detection based on luminescence resonance energy transfer between the NaYF4:Yb, Er upconversion nanoparticles and gold nanoparticles. *J. Photochem. Photobiol. A Chem.* **2020**, *389*, 112259. [CrossRef]
55. Zhou, Y.; Shao, X.; Han, Y.; Zhang, H. Detection of procalcitonin (PCT) using the double antibody sandwich method based on fluorescence resonance energy transfer between upconversion nanoparticles and quantum dots. *Anal. Methods* **2018**, *10*, 1015–1022. [CrossRef]
56. Tan, H.; Gong, G.; Xie, S.; Song, Y.; Zhang, C.; Li, N.; Zhang, D.; Xu, L.; Xu, J.; Zheng, J. Upconversion Nanoparticles@Carbon Dots@Meso-SiO_2 Sandwiched Core–Shell Nanohybrids with Tunable Dual-Mode Luminescence for 3D Anti-Counterfeiting Barcodes. *Langmuir* **2019**, *35*, 11503–11511. [CrossRef] [PubMed]
57. Chen, M.; Hassan, M.; Li, H.; Chen, Q. Fluorometric determination of lead(II) by using aptamer-functionalized upconversion nanoparticles and magnetite-modified gold nanoparticles. *Mikrochim. Acta* **2020**, *187*, 85. [CrossRef]
58. Hu, J.; Wang, R.; Fan, R.; Huang, Z.; Liu, Y.; Guo, G.; Fu, H. Enhanced luminescence in Yb3+ doped core-shell upconversion nanoparticles for sensitive doxorubicin detection. *J. Lumin.* **2020**, *217*, 116812. [CrossRef]
59. Yan, Z.; Fang, G.-Z. Molecularly imprinted polymer based on upconversion nanoparticles for highly selective and sensitive determination of Ochratoxin A. *J. Central South Univ.* **2019**, *26*, 515–523. [CrossRef]
60. Tang, Y.; Liu, H.; Gao, J.; Liu, X.; Gao, X.; Lu, X.; Fang, G.; Wang, J.; Li, J. Upconversion particle@Fe3O4@molecularly imprinted polymer with controllable shell thickness as high-performance fluorescent probe for sensing quinolones. *Talanta* **2018**, *181*, 95–103. [CrossRef] [PubMed]

61. Jin, X.; Fang, G.; Pan, M.; Yang, Y.; Bai, X.; Wang, S. A molecularly imprinted electrochemiluminescence sensor based on upconversion nanoparticles enhanced by electrodeposited rGO for selective and ultrasensitive detection of clenbuterol. *Biosens. Bioelectron.* **2018**, *102*, 357–364. [CrossRef] [PubMed]
62. Demirçalı, A. Novel heterocyclic disazo dyes containing pyrazole and phenylpyrazole. part 1: Synthesis, characterization, solvent polarity and acid-base sensitive characteristics. *J. Mol. Struct.* **2021**, *1231*, 129960. [CrossRef]
63. Levina, E.N. Fluorescein-labeled antibodies in detection of Bacillus anthracis. I. *J. Microbiol. Epidemiol. Immunobiol.* **1958**, *29*, 9–15.
64. Guan, Y.; Qu, S.; Li, B.; Zhang, L.; Ma, H.; Zhang, L. Ratiometric fluorescent nanosensors for selective detecting cysteine with upconversion luminescence. *Biosens. Bioelectron.* **2016**, *77*, 124–130. [CrossRef]
65. Zhang, H.; Fang, C.; Wu, S.; Duan, N.; Wang, Z. Upconversion luminescence resonance energy transfer-based aptasensor for the sensitive detection of oxytetracycline. *Anal. Biochem.* **2015**, *489*, 44–49. [CrossRef]
66. Liu, X.; Ren, J.; Su, L.; Gao, X.; Tang, Y.; Ma, T.; Zhu, L.; Li, J. Novel hybrid probe based on double recognition of aptamer-molecularly imprinted polymer grafted on upconversion nanoparticles for enrofloxacin sensing. *Biosens. Bioelectron.* **2017**, *87*, 203–208. [CrossRef]
67. Tenga, B.; Dingbc, B.; Shaob, S.; Wangd, Z.; Tonga, W.; Wanga, S.; Chengbc, Z.; Linbc, J.; Ping'Anmaabc, P. Intracellular RNA and nuclear DNA-dual-targeted tumor therapy via upconversion nanoplatforms with UCL/MR dual-mode bioimaging. *Chem. Eng. J.* **2020**, *405*, 126606. [CrossRef]
68. Tsai, E.S.; Himmelstoß, S.F.; Wiesholler, L.M.; Hirsch, T.; Hall, E.A.H. Upconversion nanoparticles for sensing pH. *Anal.* **2019**, *144*, 5547–5557. [CrossRef] [PubMed]
69. Zhou, J.-C.; Yang, Z.-L.; Dong, W.; Tang, R.-J.; Sun, L.-D.; Yan, C.-H. Bioimaging and toxicity assessments of near-infrared upconversion luminescent NaYF4:Yb,Tm nanocrystals. *Biomaterials* **2011**, *32*, 9059–9067. [CrossRef]
70. Liu, M.; Zhang, L.; Jiang, S.; Fu, Z. A facile luminescence resonance energy transfer method for detecting cyano-containing pesticides in herbal medicines. *Microchem. J.* **2019**, *152*, 104451. [CrossRef]
71. Liu, C.; Wang, H.; Li, X.; Chen, D. Monodisperse, size-tunable and highly efficient β-NaYF4:Yb,Er(Tm) up-conversion luminescent nanospheres: Controllable synthesis and their surface modifications. *J. Mater. Chem.* **2009**, *19*, 3546–3553. [CrossRef]
72. Liu, M.; Wei, J.; Wang, Y.; Ouyang, H.; Fu, Z. Dopamine-functionalized upconversion nanoparticles as fluorescent sensors for organophosphorus pesticide analysis. *Talanta* **2018**, *195*, 706–712. [CrossRef]
73. You, M.; Lin, M.; Wang, S.; Wang, X.; Zhang, G.; Hong, Y.; Dong, Y.; Jin, G.; Xu, F. Three-dimensional quick response code based on inkjet printing of upconversion fluorescent nanoparticles for drug anti-counterfeiting. *Nanoscale* **2016**, *8*, 10096–10104. [CrossRef]
74. Zhang, Z.; Ma, X.; Geng, Z.; Wang, K.; Wang, Z. One-step synthesis of carboxyl-functionalized rare-earth fluoride nanoparticles for cell imaging and drug delivery. *RSC Adv.* **2015**, *5*, 33999–34007. [CrossRef]
75. Wang, M.; Zhang, T.; Hu, Y.; Qin, Y.; Wei, W. In Situ Synthesis of Dicarboxylic Acid Functionalized Upconversion Nanoparticles for Bioimaging Applications. *ChemPhotoChem* **2018**, *3*, 145–150. [CrossRef]
76. Sheng, W.; Duan, W.; Shi, Y.; Chang, Q.; Zhang, Y.; Lu, Y.; Wang, S. Sensitive detection of bisphenol A in drinking water and river water using an upconversion nanoparticles-based fluorescence immunoassay in combination with magnetic separation. *Anal. Methods* **2018**, *10*, 5313–5320. [CrossRef]
77. Chen, Y.; D'Amario, C.; Gee, A.; Duong, H.T.; Shimoni, O.; Valenzuela, S.M. Dispersion stability and biocompatibility of four ligand-exchanged NaYF4: Yb, Er upconversion nanoparticles. *Acta Biomater.* **2019**, *102*, 384–393. [CrossRef] [PubMed]
78. Deng, H.; Huang, S.; Xu, C. Intensely red-emitting luminescent upconversion nanoparticles for deep-tissue multimodal bioimaging. *Talanta* **2018**, *184*, 461–467. [CrossRef] [PubMed]
79. Wang, X.; Yang, J.; Sun, X.; Yu, H.; Yan, F.; Meguellati, K.; Cheng, Z.; Zhang, H.; Yang, Y.-W. Facile surface functionalization of upconversion nanoparticles with phosphoryl pillar[5]arenes for controlled cargo release and cell imaging. *Chem. Commun.* **2018**, *54*, 12990–12993. [CrossRef] [PubMed]
80. Ni, J.; Shan, C.; Li, B.; Zhang, L.; Ma, H.; Luo, Y.; Song, H. Assembling of a functional cyclodextrin-decorated upconversion luminescence nanoplatform for cysteine-sensing. *Chem. Commun.* **2015**, *51*, 14054–14056. [CrossRef]
81. Hu, H.; Yu, M.; Li, F.; Chen, Z.; Gao, X.; Xiong, L.; Huang, C. Facile Epoxidation Strategy for Producing Amphiphilic Up-Converting Rare-Earth Nanophosphors as Biological Labels. *Chem. Mater.* **2008**, *20*, 7003–7009. [CrossRef]
82. Bai, X.; Xu, S.; Liu, J.; Wang, L. Upconversion luminescence tracking of gene delivery via multifunctional nanocapsules. *Talanta* **2016**, *150*, 118–124. [CrossRef] [PubMed]
83. Gu, B.; Zhou, Y.; Zhang, X.; Liu, X.; Zhang, Y.; Marks, R.; Zhang, H.; Zhang, Q. Thiazole derivative-modified upconversion nanoparticles for Hg^{2+} detection in living cells. *Nanoscale* **2015**, *8*, 276–282. [CrossRef] [PubMed]
84. Hao, S.; Chen, G.; Yang, C. Sensing Using Rare-Earth-Doped Upconversion Nanoparticles. *Theranostics* **2013**, *3*, 331–345. [CrossRef]
85. Singh, R.; Dumlupinar, G.; Andersson-Engels, S.; Melgar, S. Emerging applications of upconverting nanoparticles in intestinal infection and colorectal cancer. *Int. J. Nanomed.* **2019**, *14*, 1027–1038. [CrossRef]
86. Xue, Z.; Zhang, Y.; Yu, W.; Zhang, J.; Wang, J.; Wan, F.; Kim, Y.; Liu, Y.; Kou, X. Recent advances in aflatoxin B1 detection based on nanotechnology and nanomaterials-A review. *Anal. Chim. Acta* **2019**, *1069*, 32. [CrossRef]

87. Liu, X.; Kong, X.; Zhang, Y.; Tu, L.; Wang, Y.; Zeng, Q.; Li, C.; Shi, Z.; Zhang, H. Breakthrough in concentration quenching threshold of upconversion luminescence via spatial separation of the emitter doping area for bio-applications. *Chem. Commun.* **2011**, *47*, 11957–11959. [CrossRef]
88. Achatz, D.E.; Ali, R.; Wolfbeis, O.S. Luminescent Chemical Sensing, Biosensing, and Screening Using Upconverting Nanoparticles. In *Luminescence Applied in Sensor Science*; Prodi, L., Montalti, M., Zaccheroni, N., Eds.; Springer: Berlin/Heidelberg, Germany, 2011; Volume 300, pp. 29–50.
89. Petrakova, V.; Benson, V.; Buncek, M.; Fiserova, A.; Ledvina, M.; Stursa, J.; Cigler, P.; Nesladek, M. Imaging of transfection and intracellular release of intact, non-labeled DNA using fluorescent nanodiamonds. *Nanoscale* **2016**, *8*, 12002–12012. [CrossRef]
90. Liu, Z.; Yang, L.; Sharma, A.S.; Chen, M.; Chen, Q. A system composed of polyethylenimine-capped upconversion nanoparticles, copper(II), hydrogen peroxide and 3,3′,5,5′-tetramethylbenzidine for colorimetric and fluorometric determination of glyphosate. *Mikrochim. Acta* **2019**, *186*, 835. [CrossRef] [PubMed]
91. Long, Q.; Fang, A.; Wen, Y.; Li, H.; Zhang, Y.; Yao, S. Rapid and highly-sensitive uric acid sensing based on enzymatic catalysis-induced upconversion inner filter effect. *Biosens. Bioelectron.* **2016**, *86*, 109–114. [CrossRef]
92. Zu, F.; Yan, F.; Bai, Z.; Xu, J.; Wang, Y.; Huang, Y.; Zhou, X. The quenching of the fluorescence of carbon dots: A review on mechanisms and applications. *Mikrochim. Acta* **2017**, *184*, 1899–1914. [CrossRef]
93. Fang, A.; Wu, Q.; Lu, Q.; Chen, H.; Li, H.; Liu, M.; Zhang, Y.; Yao, S. Upconversion ratiometric fluorescence and colorimetric dual-readout assay for uric acid. *Biosens. Bioelectron.* **2016**, *86*, 664–670. [CrossRef]
94. Tan, C.; Atas, E.; Müller, J.G.; Pinto, M.R.; Kleiman, V.D.; Schanze, K.S. Amplified Quenching of a Conjugated Polyelectrolyte by Cyanine Dyes. *J. Am. Chem. Soc.* **2004**, *126*, 13685–13694. [CrossRef] [PubMed]
95. Kang, D.; Jeon, E.; Kim, S.; Lee, J. Lanthanide-Doped Upconversion Nanomaterials: Recent Advances and Applications. *BioChip J.* **2020**, *14*, 124–135. [CrossRef]
96. Guo, Y.; Zhao, W. Nanomaterials for luminescent detection of water and humidity. *Analyst* **2018**, *144*, 388–395. [CrossRef] [PubMed]
97. Zhang, Z.; Shikha, S.; Liu, J.; Zhang, J.; Mei, Q.; Zhang, Y. Upconversion Nanoprobes: Recent Advances in Sensing Applications. *Anal. Chem.* **2018**, *91*, 548–568. [CrossRef] [PubMed]
98. Saleh, S.M.; Alminderej, F.M.; Ali, R.; Abdallah, O.I. Optical sensor film for metribuzin pesticide detection. *Spectrochim. Acta Part A Mol. Biomol. Spectrosc.* **2019**, *229*, 117971. [CrossRef] [PubMed]
99. Li, Q.; Bai, J.; Ren, S.; Wang, J.; Gao, Y.; Li, S.; Peng, Y.; Ning, B.; Gao, Z. An ultrasensitive sensor based on quantitatively modified upconversion particles for trace bisphenol A detection. *Anal. Bioanal. Chem.* **2018**, *411*, 171–179. [CrossRef]
100. Guo, X.; Wu, S.; Duan, N.; Wang, Z. Mn2+-doped NaYF4:Yb/Er upconversion nanoparticle-based electrochemiluminescent aptasensor for bisphenol A. *Anal. Bioanal. Chem.* **2016**, *408*, 3823–3831. [CrossRef]
101. Li, J.; Liu, L.; Guo, H.Q.; Lin, L.K.; Hu, S.Y.; Ruan, J.J.; Liu, W.S.; Yan, L.S.; Li, K.X. An Upconversion Fluorescent Method for Rapid Detection of Perfluorooctane Sulfonate in Water Samples Based on Fluorine-Fluorine Interaction. *Chin. J. Anal. Chem.* **2019**, *47*, 380–387. [CrossRef]
102. Wang, Y.; Bai, J.; Huo, B.; Yuan, S.; Zhang, M.; Sun, X.; Peng, Y.; Li, S.; Wang, J.; Ning, B.; et al. Upconversion Fluorescent Aptasensor for Polychlorinated Biphenyls Detection Based on Nicking Endonuclease and Hybridization Chain Reaction Dual-Amplification Strategy. *Anal. Chem.* **2018**, *90*, 9936–9942. [CrossRef]
103. He, L.; Yang, L.; Zhu, H.; Dong, W.; Ding, Y.; Zhu, J.-J. A highly sensitive biosensing platform based on upconversion nanoparticles and graphene quantum dots for the detection of Ag^{+}. *Methods Appl. Fluoresc.* **2017**, *5*, 024010. [CrossRef] [PubMed]
104. Liu, S.; Li, Y.; Zhang, C.; Yang, L.; Zhao, T.; Zhang, R.; Jiang, C. Upconversion color tuning in Ce3+-doped LiYF4:Yb3+/Ho3+@LiYF4 nanoparticles towards ratiometric fluorescence detection of chromium(III). *J. Colloid Interface Sci.* **2017**, *493*, 10–16. [CrossRef]
105. Chen, M.; Kutsanedzie, F.Y.H.; Cheng, W.; Agyekum, A.A.; Li, H.; Chen, Q. A nanosystem composed of upconversion nanoparticles and N, N-diethyl-p-phenylenediamine for fluorimetric determination of ferric ion. *Mikrochim. Acta* **2018**, *185*, 378. [CrossRef] [PubMed]
106. Chien, H.-W.; Wu, C.-H.; Yang, C.-H.; Wang, T.-L. Multiple doping effect of LiYF4:Yb3+/Er3+/Ho3+/Tm3+@LiYF4:Yb3+ core/shell nanoparticles and its application in Hg2+ sensing detection. *J. Alloys Compd.* **2019**, *806*, 272–282. [CrossRef]
107. Wang, Y.; Lv, M.; Chen, Z.; Deng, Z.; Liu, N.; Fan, J.; Zhang, W. A Fluorescence Resonance Energy Transfer Probe Based on DNA-Modified Upconversion and Gold Nanoparticles for Detection of Lead Ions. *Front. Chem.* **2020**, *8*, 238. [CrossRef] [PubMed]
108. Shao, H.; Ma, Q.; Yu, W.; Dong, X.; Hong, X. "Off-On" typed upconversion fluorescence resonance energy transfer probe for the determination of Cu2+ in tap water. *Spectrochim. Acta Part A Mol. Biomol. Spectrosc.* **2022**, *271*, 120920. [CrossRef]
109. Ramírez-García, G.; Cervantes, E.D.; Mounzer, O.; De la Rosa, E.; Luke, T.L.; de la Cruz, F.N. A Turn-On Luminescence Method for Phosphate Determination Based on Fast Green-Functionalized ZrO_2:Yb,Er@ZrO_2Core@Shell Upconversion Nanoparticles. *Anal. Chem.* **2019**, *91*, 14657–14665. [CrossRef] [PubMed]
110. Zhang, C.; Ling, X.; Mei, Q.; He, H.; Deng, S.; Zhang, Y. Surface lanthanide activator doping for constructing highly efficient energy transfer-based nanoprobes for the on-site monitoring of atmospheric sulfur dioxide. *Analyst* **2019**, *145*, 537–543. [CrossRef]
111. Tian, L.; Guo, H.; Li, J.; Yan, L.; Zhu, E.; Liu, X.; Li, K. Fabrication of a near-infrared excitation surface molecular imprinting ratiometric fluorescent probe for sensitive and rapid detecting perfluorooctane sulfonate in complex matrix. *J. Hazard. Mater.* **2021**, *413*, 125353. [CrossRef]

112. Ge, X.; Wei, R.; Sun, L. Lanthanide nanoparticles with efficient near-infrared-II emission for biological applications. *J. Mater. Chem. B* **2020**, *8*, 10257–10270. [CrossRef] [PubMed]
113. Li, Z.; Ding, X.; Cong, H.; Wang, S.; Yu, B.; Shen, Y. Recent advances on inorganic lanthanide-doped NIR-II fluorescence nanoprobes for bioapplication. *J. Lumin.* **2020**, *228*, 117627. [CrossRef]
114. Long, Q.; Zhao, J.; Yin, B.; Li, H.; Zhang, Y.; Yao, S. A novel label-free upconversion fluorescence resonance energy transfer-nanosensor for ultrasensitive detection of protamine and heparin. *Anal. Biochem.* **2015**, *477*, 28–34. [CrossRef] [PubMed]
115. Liu, Z.; Yang, B.; Chen, B.; He, M.; Hu, B. Upconversion nanoparticle as elemental tag for the determination of alpha-fetoprotein in human serum by inductively coupled plasma mass spectrometry. *Analyst* **2016**, *142*, 197–205. [CrossRef] [PubMed]
116. Zhai, Y.; Liu, D.; Jiang, Y.; Chen, X.; Shao, L.; Li, J.; Sheng, K.; Zhang, X.; Song, H. Near-infrared-light-triggered photoelectrochemical biosensor for detection of alpha-fetoprotein based on upconversion nanophosphors. *Sens. Actuators B Chem.* **2019**, *286*, 468–475. [CrossRef]
117. Luo, Z.; Zhang, L.; Zeng, R.; Su, L.; Tang, D. Near-Infrared Light-Excited Core–Core–Shell UCNP@Au@CdS Upconversion Nanospheres for Ultrasensitive Photoelectrochemical Enzyme Immunoassay. *Anal. Chem.* **2018**, *90*, 9568–9575. [CrossRef]
118. Liu, Y.; Liu, W.-J.; Hu, J.; Li, Y.; Wang, Y.; Zhao, L.-X. Affinity binding-mediated fluorometric protein assay based on the use of target-triggered DNA assembling probes and aptamers labelled with upconversion nanoparticles: Application to the determination of platelet derived growth factor-BB. *Mikrochim. Acta* **2019**, *187*, 9. [CrossRef]
119. Chen, H.; Pang, X.; Ni, Z.; Liu, M.; Zhang, Y.; Yao, S. Upconversion nanoparticles with bright red luminescence for highly sensitive quantifying alkaline phosphatase activity based on target-triggered fusing reaction. *Anal. Chim. Acta* **2019**, *1095*, 146–153. [CrossRef]
120. Liang, M.-Y.; Zhao, B.; Xiong, Y.; Chen, W.-X.; Huo, J.-Z.; Zhang, F.; Wang, L.; Li, Y. A "turn-on" sensor based on MnO_2coated UCNPs for detection of alkaline phosphatase and ascorbic acid. *Dalton Trans.* **2019**, *48*, 16199–16210. [CrossRef]
121. Fang, A.; Chen, H.; Li, H.; Liu, M.; Zhang, Y.; Yao, S. Glutathione regulation-based dual-functional upconversion sensing-platform for acetylcholinesterase activity and cadmium ions. *Biosens. Bioelectron.* **2017**, *87*, 545–551. [CrossRef]
122. Wu, J.; Wang, H.; Yang, H.; Chen, J.; Yang, H. A novel arginine bioprobe based on up-conversion fluorescence resonance energy transfer. *Anal. Chim. Acta* **2019**, *1079*, 200–206. [CrossRef] [PubMed]
123. Wang, H.; Lu, Y.; Wang, L.; Chen, H. Detection of tyramine and tyrosinase activity using red region emission NaGdF4:Yb,Er@NaYF4 upconversion nanoparticles. *Talanta* **2019**, *197*, 558–566. [CrossRef] [PubMed]
124. Nguyen, T.-T.T.; Huy, B.T.; Tawfik, S.M.; Zayakhuu, G.; Cho, H.H.; Lee, Y.-I. Highly selective and sensitive optosensing of glutathione based on fluorescence resonance energy transfer of upconversion nanoparticles coated with a Rhodamine B derivative. *Arab. J. Chem.* **2020**, *13*, 2671–2679. [CrossRef]
125. Chen, B.; Wang, F. $NaYbF_4$@CaF_2 core–satellite upconversion nanoparticles: One-pot synthesis and sensitive detection of glutathione. *Nanoscale* **2018**, *10*, 19898–19905. [CrossRef]
126. Pulgarín, J.A.M.; Molina, A.A.; García, E.J.; Gómez, L.G. A sensitive resonance Rayleigh scattering sensor for dopamine in urine using upconversion nanoparticles. *J. Raman Spectrosc.* **2019**, *51*, 406–413. [CrossRef]
127. Kumar, B.; Murali, A.; Giri, S. Upconversion Nanoplatform for FRET-Based Sensing of Dopamine and pH. *ChemistrySelect* **2019**, *4*, 5407–5414. [CrossRef]
128. Liu, J.; Yu, C.; Han, L.; Shen, Y.; Fang, Y.; Xia, Y.; Yao, X.; Wu, F.; Li, C.; Chen, J.; et al. Upconversion luminescence–based aptasensor for the detection of thyroid-stimulating hormone in serum. *Mikrochim. Acta* **2022**, *189*, 179. [CrossRef]
129. Gao, R.; Hao, C.; Xu, L.; Xu, C.; Kuang, H. Spiny Nanorod and Upconversion Nanoparticle Satellite Assemblies for Ultrasensitive Detection of Messenger RNA in Living Cells. *Anal. Chem.* **2018**, *90*, 5414–5421. [CrossRef]
130. Liu, X.; Zhang, S.-Q.; Cheng, Z.-H.; Wei, X.; Yang, T.; Yu, Y.-L.; Chen, M.-L.; Wang, J.-H. Highly Sensitive Detection of MicroRNA-21 with ICPMS via Hybridization Accumulation of Upconversion Nanoparticles. *Anal. Chem.* **2018**, *90*, 12116–12122. [CrossRef]
131. Zhu, D.; Miao, Z.Y.; Hu, Y.; Zhang, X.J. Single-step, homogeneous and sensitive detection for microRNAs with dual-recognition steps based on luminescence resonance energy transfer (LRET) using upconversion nanoparticles. *Biosens. Bioelectron.* **2017**, *100*, 475–481. [CrossRef]
132. Chen, F.; Lu, Q.; Zhang, Y.; Yao, S. Strand displacement dual amplification miRNAs strategy with FRET between NaYF4:Yb,Tm/Er upconversion nanoparticles and Ti3C2 nanosheets. *Sensors Actuators B Chem.* **2019**, *297*, 126751. [CrossRef]
133. Gu, T.; Ren, Z.; Li, X.; Huang, J.; Han, G. A flexible smart membrane consisting of GO composite fibres and upconversion MSNs for microRNA detection. *Chem. Commun.* **2019**, *55*, 9104–9107. [CrossRef] [PubMed]
134. Jiang, X.; Hao, C.; Zhang, H.; Wu, X.; Xu, L.; Sun, M.; Xu, C.; Kuang, H. Dual-Modal Fe_xCu_ySe and Upconversion Nanoparticle Assemblies for Intracellular MicroRNA-21 Detection. *ACS Appl. Mater. Interfaces* **2020**, *13*, 41405–41413. [CrossRef] [PubMed]
135. Cheng, Z.-H.; Liu, X.; Zhang, S.-Q.; Yang, T.; Chen, M.-L.; Wang, J.-H. Placeholder Strategy with Upconversion Nanoparticles−Eriochrome Black T Conjugate for a Colorimetric Assay of an Anthrax Biomarker. *Anal. Chem.* **2019**, *91*, 12094–12099. [CrossRef]
136. Chen, Q.; Hu, W.; Sun, C.; Li, H.; Ouyang, Q. Synthesis of improved upconversion nanoparticles as ultrasensitive fluorescence probe for mycotoxins. *Anal. Chim. Acta* **2016**, *938*, 137–145. [CrossRef] [PubMed]
137. Jin, B.; Wang, S.; Lin, M.; Jin, Y.; Zhang, S.; Cui, X.; Gong, Y.; Li, A.; Xu, F.; Lu, T.J. Upconversion nanoparticles based FRET aptasensor for rapid and ultrasenstive bacteria detection. *Biosens. Bioelectron.* **2017**, *90*, 525–533. [CrossRef] [PubMed]
138. Li, H.; Ahmad, W.; Rong, Y.; Chen, Q.; Zuo, M.; Ouyang, Q.; Guo, Z. Designing an aptamer based magnetic and upconversion nanoparticles conjugated fluorescence sensor for screening Escherichia coli in food. *Food Control* **2019**, *107*, 106761. [CrossRef]

139. Wang, P.; Wang, A.; Hassan, M.; Ouyang, Q.; Li, H.; Chen, Q. A highly sensitive upconversion nanoparticles-WS2 nanosheet sensing platform for *Escherichia coli* detection. *Sens. Actuators B Chem.* **2020**, *320*, 128434. [CrossRef]
140. He, D.; Wu, Z.; Cui, B.; Jin, Z.; Xu, E. A fluorometric method for aptamer-based simultaneous determination of two kinds of the fusarium mycotoxins zearalenone and fumonisin B1 making use of gold nanorods and upconversion nanoparticles. *Mikrochim. Acta* **2020**, *187*, 179. [CrossRef] [PubMed]
141. Lv, J.; Zhao, S.; Wu, S.; Wang, Z. Upconversion nanoparticles grafted molybdenum disulfide nanosheets platform for microcystin-LR sensing. *Biosens. Bioelectron.* **2017**, *90*, 203–209. [CrossRef] [PubMed]
142. Liao, Z.; Zhang, Y.; Su, L.; Chang, J.; Wang, H. Application of upconversion luminescent-magnetic microbeads with weak background noise and facile separation in ochratoxin A detection. *J. Nanoparticle Res.* **2017**, *19*, 1–12. [CrossRef]
143. Wu, S.; Liu, L.; Duan, N.; Wang, W.; Yu, Q.; Wang, Z. A test strip for ochratoxin A based on the use of aptamer-modified fluorescence upconversion nanoparticles. *Mikrochim. Acta* **2018**, *185*, 497. [CrossRef] [PubMed]
144. Kim, K.; Jo, E.-J.; Lee, K.J.; Park, J.; Jung, G.Y.; Shin, Y.-B.; Lee, L.P.; Kim, M.-G. Gold nanocap-supported upconversion nanoparticles for fabrication of a solid-phase aptasensor to detect ochratoxin A. *Biosens. Bioelectron.* **2019**, *150*, 111885. [CrossRef]
145. Yang, M.; Cui, M.; Wang, W.; Yang, Y.; Chang, J.; Hao, J.; Wang, H. Background-free upconversion-encoded microspheres for mycotoxin detection based on a rapid visualization method. *Anal. Bioanal. Chem.* **2020**, *412*, 81–91. [CrossRef]
146. Sun, M.; Qu, A.; Hao, C.; Wu, X.; Xu, L.; Xu, C.; Kuang, H. Chiral Upconversion Heterodimers for Quantitative Analysis and Bioimaging of Antibiotic-Resistant Bacteria In Vivo. *Adv. Mater.* **2018**, *30*, e1804241. [CrossRef]
147. Xin, H.; Li, Y.; Xu, D.; Zhang, Y.; Chen, C.-H.; Li, B. Single Upconversion Nanoparticle-Bacterium Cotrapping for Single-Bacterium Labeling and Analysis. *Small* **2017**, *13*, 3418. [CrossRef]
148. Wu, Z.; He, D.; Cui, B. A fluorometric assay for staphylococcal enterotoxin B by making use of platinum coated gold nanorods and of upconversion nanoparticles. *Mikrochim. Acta* **2018**, *185*, 516. [CrossRef]
149. Wu, Z.; He, D.; Cui, B.; Jin, Z.; Xu, E. Triple-Mode Aptasensor for Sensitive and Reliable Determination of Staphylococcal Enterotoxin B. *Food Anal. Methods* **2020**, *13*, 1255–1261. [CrossRef]
150. Zhao, Y.; Zhang, P.; Wang, J.; Zhou, L.; Yang, R. A novel electro-driven immunochromatography assay based on upconversion nanoparticles for rapid pathogen detection. *Biosens. Bioelectron.* **2020**, *152*, 112037. [CrossRef] [PubMed]
151. Liu, R.; Zhang, Y.; Ali, S.; Haruna, S.A.; He, P.; Li, H.; Ouyang, Q.; Chen, Q. Development of a fluorescence aptasensor for rapid and sensitive detection of Listeria monocytogenes in food. *Food Control* **2020**, *122*, 107808. [CrossRef]
152. Ouyang, Q.; Yang, Y.; Ali, S.; Wang, L.; Li, H.; Chen, Q. Upconversion nanoparticles-based FRET system for sensitive detection of Staphylococcus aureus. *Spectrochim. Acta Part A Mol. Biomol. Spectrosc.* **2021**, *255*, 119734. [CrossRef]
153. Wei, R.; Wei, Z.; Sun, L.; Zhang, J.Z.; Liu, J.; Ge, X.; Shi, L. Nile Red Derivative-Modified Nanostructure for Upconversion Luminescence Sensing and Intracellular Detection of Fe^{3+} and MR Imaging. *ACS Appl. Mater. Interfaces* **2015**, *8*, 400–410. [CrossRef] [PubMed]
154. Zhao, M.; Xu, F.; Wang, L.; Chen, H. A single-particle enumeration method for the detection of Fe2+ based on a near-infrared core–shell upconversion nanoparticle and IR-808 dye composite nanoprobe. *Analyst* **2019**, *145*, 530–536. [CrossRef] [PubMed]
155. Jiang, M.; Xu, S.; Yu, Y.; Gao, Y.; Yin, Z.; Li, J.; Zhang, X.; Yu, H.; Chen, B. Turn-on fluorescence ferrous ions detection based on MnO2 nanosheets modified upconverion nanoparticles. *Spectrochim. Acta Part A Mol. Biomol. Spectrosc.* **2021**, *264*, 120275. [CrossRef]
156. Huang, X.; Liu, Q.; Yao, S.; Jiang, G. Recent progress in the application of nanomaterials in the analysis of emerging chemical contaminants. *Anal. Methods* **2017**, *9*, 2768–2783. [CrossRef]
157. Pirovano, P.; Dorrian, M.; Shinde, A.; Donohoe, A.; Brady, A.J.; Moyna, N.M.; Wallace, G.; Diamond, D.; McCaul, M. A wearable sensor for the detection of sodium and potassium in human sweat during exercise. *Talanta* **2020**, *219*, 121145. [CrossRef]
158. Iannazzo, D.; Espro, C.; Ferlazzo, A.; Celesti, C.; Branca, C.; Neri, G. Electrochemical and Fluorescent Properties of Crown Ether Functionalized Graphene Quantum Dots for Potassium and Sodium Ions Detection. *Nanomaterials* **2021**, *11*, 2897. [CrossRef] [PubMed]
159. Chen, F.; Lu, Q.; Huang, L.; Liu, B.; Liu, M.; Zhang, Y.; Liu, J. DNA Triplex and Quadruplex Assembled Nanosensors for Correlating K^+ and pH in Lysosomes. *Angew. Chem. Int. Ed.* **2020**, *60*, 5453–5458. [CrossRef]
160. Hao, C.; Wu, X.; Sun, M.; Zhang, H.; Yuan, A.; Xu, L.; Xu, C.; Kuang, H. Chiral Core–Shell Upconversion Nanoparticle@MOF Nanoassemblies for Quantification and Bioimaging of Reactive Oxygen Species *in Vivo*. *J. Am. Chem. Soc.* **2019**, *141*, 19373–19378. [CrossRef]
161. Zou, X.; Zhou, X.; Cao, C.; Lu, W.; Yuan, W.; Liu, Q.; Feng, W.; Li, F. Dye-sensitized upconversion nanocomposites for ratiometric semi-quantitative detection of hypochlorite *in vivo*. *Nanoscale* **2019**, *11*, 2959–2965. [CrossRef]
162. Chen, H.; Lu, Q.; He, K.; Liu, M.; Zhang, Y.; Yao, S. A cyclic signal amplification strategy to fluorescence and colorimetric dual-readout assay for the detection of H2O2-related analytes and application to colorimetric logic gate. *Sensors Actuators B Chem.* **2018**, *260*, 908–917. [CrossRef]
163. Singh, P.; Singh, P.; Prakash, R.; Rai, S.B. Photo-physical studies of ultrasmall upconversion nanoparticles embedded organometallic complexes: Probing a dual mode optical sensor for hydrogen peroxide. *Opt. Mater.* **2019**, *98*, 109459. [CrossRef]
164. Wang, H.; Li, Y.; Yang, M.; Wang, P.; Gu, Y. FRET-Based Upconversion Nanoprobe Sensitized by Nd^{3+} for the Ratiometric Detection of Hydrogen Peroxide in Vivo. *ACS Appl. Mater. Interfaces* **2019**, *11*, 7441–7449. [CrossRef] [PubMed]

165. Yuan, A.; Hao, C.; Wu, X.; Sun, M.; Qu, A.; Xu, L.; Kuang, H.; Xu, C. Chiral Cu $_x$OS@ZIF-8 Nanostructures for Ultrasensitive Quantification of Hydrogen Sulfide In Vivo. *Adv. Mater.* **2020**, *32*, e1906580. [CrossRef] [PubMed]
166. Chen, H.; Wang, W.; Ji, C.; Wang, L. Dye-sensitized core–shell NaGdF4:Yb,Er@NaGdF4:Yb,Nd upconversion nanoprobe for determination of H2S. *Spectrochim. Acta Part A Mol. Biomol. Spectrosc.* **2020**, *248*, 119281. [CrossRef] [PubMed]
167. Wang, F.; Zhang, C.; Qu, X.; Cheng, S.; Xian, Y. Cationic cyanine chromophore-assembled upconversion nanoparticles for sensing and imaging H2S in living cells and zebrafish. *Biosens. Bioelectron.* **2018**, *126*, 96–101. [CrossRef] [PubMed]
168. Liu, Y.; Jia, Q.; Zhai, X.; Mao, F.; Jiang, A.; Zhou, J. Rationally designed pure-inorganic upconversion nanoprobes for ultra-highly selective hydrogen sulfide imaging and elimination *in vivo*. *Chem. Sci.* **2018**, *10*, 1193–1200. [CrossRef]
169. Zhou, Y.; Ling, B.; Chen, H.; Wang, L. Mn2+-doped NaYF4:Yb,Er upconversion nanoparticles for detection of uric acid based on the Fenton reaction. *Talanta* **2018**, *180*, 120–126. [CrossRef]
170. Mo, J.; Shen, L.; Xu, Q.; Zeng, J.; Sha, J.; Hu, T.; Bi, K.; Chen, Y. An Nd3+-Sensitized Upconversion Fluorescent Sensor for Epirubicin Detection. *Nanomaterials* **2019**, *9*, 1700. [CrossRef]
171. Lee, S.H.; Tawfik, S.M.; Thangadurai, D.T.; Lee, Y.-I. Highly sensitive and selective detection of Alprenolol using upconversion nanoparticles functionalized with amphiphilic conjugated polythiophene. *Microchem. J.* **2021**, *164*, 106010. [CrossRef]
172. Giust, D.; Lucío, M.I.; El-Sagheer, A.H.; Brown, T.; Williams, L.E.; Muskens, O.L.; Kanaras, A.G. Graphene Oxide–Upconversion Nanoparticle Based Portable Sensors for Assessing Nutritional Deficiencies in Crops. *ACS Nano* **2018**, *12*, 6273–6279. [CrossRef]
173. Modlitbová, P.; Hlaváček, A.; Švestková, T.; Pořízka, P.; Šimoníková, L.; Novotný, K.; Kaiser, J. The effects of photon-upconversion nanoparticles on the growth of radish and duckweed: Bioaccumulation, imaging, and spectroscopic studies. *Chemosphere* **2019**, *225*, 723–734. [CrossRef]
174. Popov, A.; Gurkov, A.; Borvinskaya, E.; Sadovoy, A.; Bykov, A.; Timofeyev, M.; Meglinski, I. Eco-photonics: Micro-encapsulated probe as implantable sensor for monitoring the physiological state of water organisms. In Proceedings of the 2018 International Conference Laser Optics (ICLO), St. Petersburg, Russia, 4–8 June 2018; p. 547. [CrossRef]
175. Yu, J.; Guo, T.; Zhang, W.; Li, B.; Liu, L.; Hua, R. Green upconversion nanoparticles for 2, 4- dichlorophenoxyacetic acid and fenitrothion detection. *J. Alloy. Compd.* **2018**, *771*, 187–194. [CrossRef]
176. Lin, X.; Yu, Q.; Yang, W.; He, C.; Zhou, Y.; Duan, N.; Wu, S. Double-enzymes-mediated fluorescent assay for sensitive determination of organophosphorus pesticides based on the quenching of upconversion nanoparticles by Fe3+. *Food Chem.* **2020**, *345*, 128809. [CrossRef] [PubMed]
177. Chen, Q.; Sheng, R.; Wang, P.; Ouyang, Q.; Wang, A.; Ali, S.; Zareef, M.; Hassan, M. Ultra-sensitive detection of malathion residues using FRET-based upconversion fluorescence sensor in food. *Spectrochim. Acta Part A Mol. Biomol. Spectrosc.* **2020**, *241*, 118654. [CrossRef] [PubMed]
178. Long, Q.; Li, H.; Zhang, Y.; Yao, S. Upconversion nanoparticle-based fluorescence resonance energy transfer assay for organophosphorus pesticides. *Biosens. Bioelectron.* **2015**, *68*, 168–174. [CrossRef] [PubMed]
179. Wang, P.; Li, H.; Hassan, M.; Guo, Z.; Zhang, Z.-Z.; Chen, Q. Fabricating an Acetylcholinesterase Modulated UCNPs-Cu^{2+} Fluorescence Biosensor for Ultrasensitive Detection of Organophosphorus Pesticides-Diazinon in Food. *J. Agric. Food Chem.* **2019**, *67*, 4071–4079. [CrossRef]
180. Rong, Y.; Li, H.; Ouyang, Q.; Ali, S.; Chen, Q. Rapid and sensitive detection of diazinon in food based on the FRET between rare-earth doped upconversion nanoparticles and graphene oxide. *Spectrochim. Acta Part A Mol. Biomol. Spectrosc.* **2020**, *239*, 118500. [CrossRef]
181. Si, F.; Zou, R.; Jiao, S.; Qiao, X.; Guo, Y.; Zhu, G. Inner filter effect-based homogeneous immunoassay for rapid detection of imidacloprid residue in environmental and food samples. *Ecotoxicol. Environ. Saf.* **2018**, *148*, 862–868. [CrossRef]
182. Sun, N.; Ding, Y.; Tao, Z.; You, H.; Hua, X.; Wang, M. Development of an upconversion fluorescence DNA probe for the detection of acetamiprid by magnetic nanoparticles separation. *Food Chem.* **2018**, *257*, 289–294. [CrossRef]
183. Yu, Q.; He, C.; Li, Q.; Zhou, Y.; Duan, N.; Wu, S. Fluorometric determination of acetamiprid using molecularly imprinted upconversion nanoparticles. *Mikrochim. Acta* **2020**, *187*, 222. [CrossRef]
184. Guo, T.; Wang, C.; Zhou, H.; Zhang, Y.; Ma, L. A multifunctional near-infrared fluorescent sensing material based on core-shell upconversion nanoparticles@magnetic nanoparticles and molecularly imprinted polymers for detection of deltamethrin. *Mikrochim. Acta* **2021**, *188*, 165. [CrossRef] [PubMed]
185. Zhao, L.; Jin, J.; Zhu, W.; Zuo, Y.; Song, Y. Detection of Pyrethroids in Food by Immunofluorescence Enhanced Method Based on Three-Layer Core-Shell Structure Upconversion Materials. *Foods* **2022**, *11*, 990. [CrossRef] [PubMed]
186. Su, D.; Zhao, X.; Yan, X.; Han, X.; Zhu, Z.; Wang, C.; Jia, X.; Liu, F.; Sun, P.; Liu, X.; et al. Background-free sensing platform for on-site detection of carbamate pesticide through upconversion nanoparticles-based hydrogel suit. *Biosens. Bioelectron.* **2021**, *194*, 113598. [CrossRef] [PubMed]
187. Ouyang, Q.; Wang, L.; Ahmad, W.; Rong, Y.; Li, H.; Hu, Y.; Chen, Q. A highly sensitive detection of carbendazim pesticide in food based on the upconversion-MnO2 luminescent resonance energy transfer biosensor. *Food Chem.* **2021**, *349*, 129157. [CrossRef] [PubMed]
188. Hu, P.; Wu, X.; Hu, S.; Chen, Z.; Yan, H.; Xi, Z.; Yu, Y.; Dai, G.; Liu, Y. Enhanced upconversion luminescence through core/shell structures and its application for detecting organic dyes in opaque fishes. *Photochem. Photobiol. Sci.* **2016**, *15*, 260–265. [CrossRef]

189. Hu, G.; Gao, S.; Han, X.; Yang, L. Comparison of Immunochromatographic Strips Using Colloidal Gold, Quantum Dots, and Upconversion Nanoparticles for Visual Detection of Norfloxacin in Milk Samples. *Food Anal. Methods* **2020**, *13*, 1069–1077. [CrossRef]
190. Zhang, Y.; Liu, R.; Hassan, M.; Li, H.; Ouyang, Q.; Chen, Q. Fluorescence resonance energy transfer-based aptasensor for sensitive detection of kanamycin in food. *Spectrochim. Acta Part A Mol. Biomol. Spectrosc.* **2021**, *262*, 120147. [CrossRef]
191. Zhang, Y.; Xu, S.; Li, X.; Zhang, J.; Sun, J.; Tong, L.; Zhong, H.; Xia, H.; Hua, R.; Chen, B. Improved LRET-based detection characters of Cu^{2+} using sandwich structured $NaYF_4$@$NaYF_4$:Er^{3+}/Yb^{3+}@$NaYF_4$ nanoparticles as energy donor. *Sensors Actuators B Chem.* **2018**, *257*, 829–838. [CrossRef]
192. Zhang, K.; Zhu, G.; Wei, Y.; Zhang, L.; Shen, Y. Engineering of an Upconversion Luminescence Sensing Platform Based on the Competition Effect for Mercury-Ion Monitoring in Green Tea. *J. Agric. Food Chem.* **2021**, *69*, 8565–8570. [CrossRef]
193. Gu, Y.; Jiang, Z.; Ren, D.; Shang, Y.; Hu, Y.; Yi, L. Electrochemiluminescence sensor based on the target recognition-induced aggregation of sensing units for Hg2+ determination. *Sensors Actuators B Chem.* **2021**, *337*, 129821. [CrossRef]
194. Liu, Y.; Ouyang, Q.; Li, H.; Zhang, Z.; Chen, Q. Development of an Inner Filter Effects-Based Upconversion Nanoparticles–Curcumin Nanosystem for the Sensitive Sensing of Fluoride Ion. *ACS Appl. Mater. Interfaces* **2017**, *9*, 18314–18321. [CrossRef] [PubMed]
195. Chen, H.; Xia, W.; Gao, Q.; Wang, L. Sensitive quantitative image analysis of bisulfite based on near-infrared upconversion luminescence total internal reflection platform. *Talanta* **2020**, *224*, 121928. [CrossRef] [PubMed]
196. Rong, Y.; Ali, S.; Ouyang, Q.; Wang, L.; Wang, B.; Chen, Q. A turn-on upconversion fluorescence sensor for acrylamide in potato chips based on fluorescence resonance energy transfer and thiol-ene Michael addition. *Food Chem.* **2021**, *351*, 129215. [CrossRef] [PubMed]
197. Wang, K.; Li, Y.; Li, H.; Yin, M.; Liu, H.; Deng, Q.; Wang, S. Upconversion fluorescent nanoparticles based-sensor array for discrimination of the same variety red grape wines. *RSC Adv.* **2019**, *9*, 7349–7355. [CrossRef] [PubMed]
198. Huang, X.; Sheng, W.; Chen, H.; Zhang, B.; Huang, N.; Wang, S. Upconversion Nanoparticles-Based Fluorescence Immunoassay for the Sensitive Detection of 2-Amino-3-methylimidazo [4,5-f] Quinoline (IQ) in Heat Processed Meat. *Sensors* **2021**, *22*, 8. [CrossRef]
199. del Barrio, M.; Cases, R.; Cebolla, V.; Hirsch, T.; de Marcos, S.; Wilhelm, S.; Galbán, J. A reagentless enzymatic fluorescent biosensor for glucose based on upconverting glasses, as excitation source, and chemically modified glucose oxidase. *Talanta* **2016**, *160*, 586–591. [CrossRef] [PubMed]
200. Ma, Y.; Liu, H.; Han, Z.; Yang, L.; Liu, J. Highly-reproducible Raman scattering of NaYF4:Yb,Er@SiO2@Ag for methylamphetamine detection under near-infrared laser excitation. *Analyst* **2015**, *140*, 5268–5275. [CrossRef] [PubMed]
201. Zhang, S.; Yao, T.; Wang, S.; Feng, R.; Chen, L.; Zhu, V.; Hu, G.; Zhang, H.; Yang, G. Upconversion luminescence nanoparticles-based immunochromatographic assay for quantitative detection of triamcinolone acetonide in cosmetics. *Spectrochim. Acta Part A Mol. Biomol. Spectrosc.* **2019**, *214*, 302–308. [CrossRef] [PubMed]